Renewable and Sustainable Energy Reviews 200 (2024) 114600

Contents lists available at ScienceDirect

Renewable and Sustainable Energy Reviews

journal homepage: www.elsevier.com/locate/rser

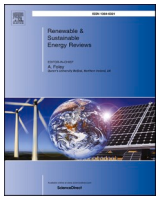

Advances and prospects in manufacturing of ceramic oxygen and hydrogen separation membranes

Simone Casadio [a,b], Angela Gondolini [a,*], Elisa Mercadelli [a,**], Alessandra Sanson [a]

[a] National Research Council of Italy, Institute of Science, Technology and Sustainability for Ceramics (CNR-ISSMC, former ISTEC) of the National Research Council (CNR), Via Granarolo 64, 48018 Faenza (RA), Italy
[b] Department of Chemical Sciences, Università degli Studi di Padova, Via Marzolo 1, 35131 Padova, Italy

ARTICLE INFO

Keywords:
Manufacturing techniques
ceramic membranes
oxygen separation
hydrogen separation

ABSTRACT

Hydrogen and oxygen are considered essential gases for industrial processes. Hydrogen is the main candidate to store discontinuous electricity produced by renewable energy sources playing a crucial role in achieving the European Green Deal goals. Ceramic membranes can supply theoretically 100 % pure gases and can be directly applied to high-temperature plants (500–900 °C). This technology shows reduced production costs, higher chemical and thermal stability compared to the precious metal-based counterparts. Despite the recent progress, challenges linked to its production processes and performances for industrial applications remain to be addressed. This review aims to give a comprehensive overview of the most used techniques and new approaches regarding the manufacturing of the most performing asymmetric (porous-dense) ceramic membranes. Oxygen separation technology is based on well-established performing materials; tangible progress is expected considering a fine-tuning of the membrane microstructure and architecture. Hydrogen separation membranes show a lower degree of advancement than the oxygen ones, suggesting the need for new materials design. For both types of membranes, one of the key requirements for industrial applications remains the manufacturing process optimization to achieve increased gas permeability and reliable components on a mass-production scale. This review offers a critical vision of the membrane technology, emphasizing the opportunities and challenges of each manufacturing method and structure. New prospects and frontier of shaping for this technology are addressed.

1. Introduction

Gas separation membranes play an important role in several industrial sectors. Hydrogen (H_2) and oxygen (O_2), represent fundamental gases for many processes and need to be efficiently separated to be used. Hydrogen is considered the most promising energy carrier and industrial feedstock in a climate-neutral economy, a target set by the European Green Deal by 2050 [1,2]. In this direction, renewable electricity can replace fossil fuels in many uses, but electrification cannot practically replace them completely in some fields (shipping, steel production, etc.). Hydrogen is the first candidate to store discontinuous electricity produced by renewable energy sources [3], playing a pivotal role in achieving the European Green Deal goals [4–6]. From this perspective, used as a source of electricity, heat, or power by means of fuel-cells technology [7], hydrogen has the potential of being effectively employed across the transport, industry, and electricity sectors, which together account for two-thirds of global CO_2 emissions [8]. Hydrogen is also important as a key molecule in several biological and biotechnological processes [9], as well as a fundamental building block for chemical commodities such as methanol (CH_3OH), ammonia (NH_3), or in the processing of intermediate oil products [10–13]. At present, it is still mostly produced from fossil fuels *via* methane steam reforming or from partial oxidation of natural gas or other hydrocarbons [14,15]. These processes lead to hydrogen in the form of syngas, a mixture mainly composed of hydrogen with variable amounts of carbon monoxide (CO) and/or carbon dioxide (CO_2) [16], and other by-products (*i.e.* water vapour, H_2S, etc.) [15]. A subsequent purification is required to separate hydrogen from other impurities avoiding carbon dioxide dispersion.

A similar discussion can likewise be extended to oxygen, which, along with hydrogen, is the most extensively employed chemicals commodity in the world [17], with many applications in almost every industrial sector (*i.e.,* gasification of carbonaceous materials [18], glass industry [19], pharmaceutical [20] and chemical industry [20], *etc.*). O_2

* Corresponding author.
** Corresponding author.
E-mail addresses: angela.gondolini@cnr.it (A. Gondolini), elisa.mercadelli@cnr.it (E. Mercadelli).

https://doi.org/10.1016/j.rser.2024.114600
Received 11 August 2023; Received in revised form 26 January 2024; Accepted 25 April 2024
Available online 1 June 2024

Abbreviations

T	temperature
NMP	N-Methyl pyrrolidone
PSA	Pressure Swing Adsorption
MIEC	Mixed Ion-Electron Conductors
BCZY	yttrium-doped barium cerate-zirconate
GDC	gadolinium doped ceria
SCY	Strontium Cerium Yttrium Oxide
SDC	samarium doped ceria
LSM	Lanthanum Strontium Manganite
YSZ	Yttrium stabilized Zirconia
LSCF	Lanthanum Strontium Cobalt Ferrite
LSCrF	Lanthanum Strontium Chromium Ferrite
PE	polyethylene
PP	polypropylene
EVA	ethylene-vinyl acetate copolymer
PSF	polysulfone
PESF	polyether sulfone
BCY	Barium Cerate Yttrium Oxide
PVA	polyvinyl alcohol

constitutes 21 % by volume of air, its separation is thus required to fulfil these industrial and medical requests.

For both H_2 and O_2, industrially applied purification technologies rely on three different alternatives, namely cryogenic distillation [20–23], Pressure Swing Adsorption (PSA) [24–28], and membrane separation. Cryogenic distillation is the most energy-demanding and operational-challenging procedure with a high capital cost due to the low temperatures (O_2: 185 °C, H_2: 252.9 °C) and high pressures required to allow partial condensation of the gas mixtures. It leads to a limited purity of the recovered gasses (O_2: ~95 % [29], H_2: 99 % [30]). PSA, relies on the selective adsorption of impurities from the gas stream operated by molecular sieve adsorbents varying the pressure. It also involves high capital-operational costs but with the significant advantage of achieving a higher purity grade (O_2: 99.5 % [29], H_2: >99.999 % [31]). This technique suffers from low H_2/O_2 recovery (~78–80 %) [32,33] owing to the pressure release during desorption. Membrane based-separation has a simple operation, small footprint (*i.e.,* more compact systems), and low capital-cost which enables the gas recovery at low energy expenses, with the additional benefits of working in continuous, ease of scalability, and low minimal treatable volumes required [34–37]. Separation membranes are attractive as essential components in advanced electrochemical systems such as catalytic membrane reactors [38–41] and solid oxide anionic [42–44] and protonic fuel cells [45–48].

Ceramic technologies for oxygen and hydrogen separation exploit the same pressure-driven mechanism of gaseous species transport and materials displaying both ionic and electronic conduction. These systems are both considered in this review for the analogous membrane architectures and fabrication processes. To the best of the author's knowledge, this is the first time that a critical analysis of the production methods to obtain asymmetric architectures of ceramic membranes has been published, as a guiding tool for the scientific community to direct their efforts and boost the commercialization of these devices. The main membrane structures and their associated production technologies are reviewed paying specific attention to innovative approaches in the gas separation membrane field.

2. Membranes for gas separation

Extensive work has been conducted on H_2 and O_2 permselective membranes, and different materials have been developed for this purpose. A prior classification of permselective membranes (see Fig. 1) can be precisely made on this basis, distinguishing between organic membranes (*i.e.,* polymeric membranes [49,50], organic/metal-organic frameworks [51]), inorganic membranes (silica membranes [52,53], zeolites [54,55], carbon-based [56], metallic [57] and ceramic [34,58,59]) and hybrid membranes (*i.e.*, composites between the first two classes).

As regard silica, zeolite, and carbon-based ones, they all consist in porous membranes whose selectivity is based on molecular sieving properties (steric-based/size exclusion separation mechanism).

Organic membranes (*i.e.,* carbon-based systems) present the intrinsic drawback of low resistance at high temperatures and pressures [60] which prevents their direct application to high-temperature industrial processes.

Inorganic membranes are, on the contrary, generally well-known for their superior chemical and thermal stability. The major drawback of any porous system is the loss of selectivity at high temperatures [61]. Metallic membranes, available for H_2, and ceramic membranes, for the separation of both H_2 and O_2, are dense systems. The hydrogen separation process is based on a solution-diffusion mechanism of H_2 [54]. The major drawback of commercially available dense metallic systems (palladium and palladium-based alloys) is their tendency to surface poisoning in CO, CO_2, unsaturated hydrocarbons, chlorine, and H_2S-containing streams, which are present in gas during operation, and that can reduce the hydrogen flux by 20 % up to 100 % [52]. The lack of mechanical resistance and high material costs, represent other disadvantages of these systems [62]. As thin membranes are required for gas separation (since the flux is inversely proportional to the film thickness), the research is nowadays mainly focused on the preparation of thin Pd films onto low-cost porous supports to provide high permeation rates maintaining good mechanical resistance and reducing material costs [52]. The operating temperature for palladium membranes is usually in the 300–500 °C range [60,63] since the exposure to hydrogen gasses at temperatures lower than 300 °C (and pressure below 2 MPa) is associated with low hydrogen permeability [64].

Dense ceramic membranes are endowed with a high thermal and chemical stability, and they are characterized by much lower material and manufacturing costs and high operating temperatures (500–900 °C). In these systems, the transport of the gaseous species follows a pressure-driven mode (*i.e.,* from the feed side at higher gas partial pressure to the permeate side at a lower gas partial pressure) in ceramic materials displaying both ionic and electronic conduction (*i.e.,* ambipolar conductors, also referred to as MIECs, *Mixed Ionic-Electronic Conductors*) [65]. Assuming the absence of any defects, the involved mechanism gives them the theoretical selectivity of 100 % [60]. Ceramic membranes are especially suitable for high-temperature gas separation (*i.e.,* industrial operational conditions), since ionic conductivity generally increases with increasing temperature [61]. The main drawback of these systems is the lower gas permeation rate compared to metal-based ones. This is due to the associated generally low electronic conductivity which limits the gas permeability to lower values. Rather than improving the ambipolar conductivity of the selected material, to overcome the intrinsic low permeability of ceramic membranes, different strategies can be adopted to maximize their permeation rate. As postulated by the Wagner's equation, in the case of fast surface exchange kinetics, the permeability of dense ceramic membranes can be increased by (i) modifying the operating conditions in terms of temperature and gas partial pressure gradient between feed and permeate side (*i.e.,* higher T and P gradient) and/or (ii) by acting on the membrane processing reducing its thickness [66–68]; the permeation rates result in fact inversely proportional to the thickness of the membrane.

In this context, an effective way to improve the performance of ceramic membranes without changing the selected materials or modifying the operating conditions is to reduce membrane thickness by adopting an asymmetric architecture. Asymmetric structures are obtained from the combination of thin dense active layers supported on

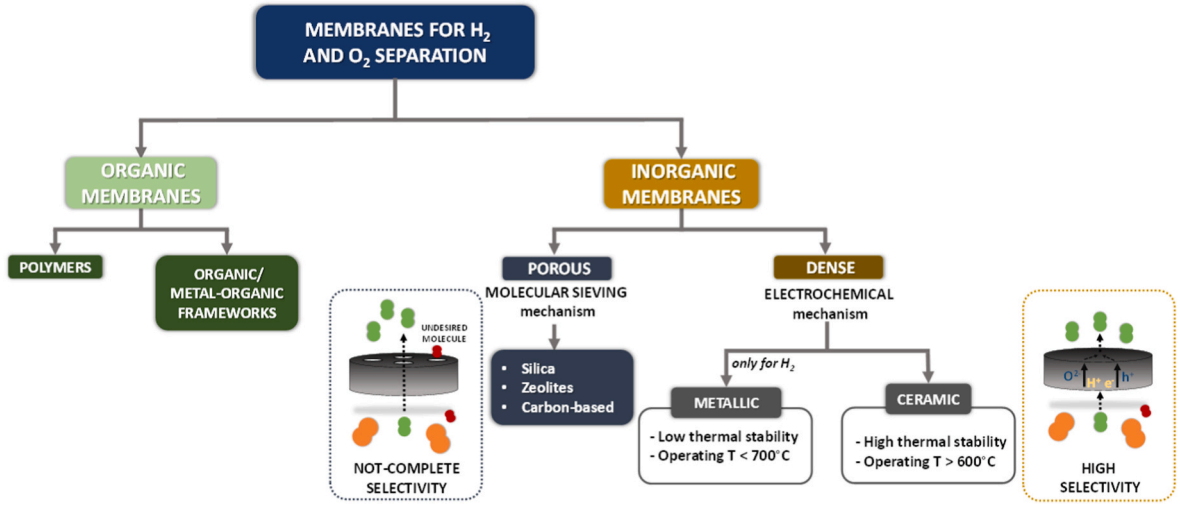

Fig. 1. Schematic diagram of gas separation membranes classification. T:temperature.

porous substrates; in this way, it is possible to overcome thickness limitation (*i.e.,* ionic bulk diffusion) without prejudicing the mechanical integrity and stability of the system. However, the successful production of asymmetric ceramic membranes represents, to date, a crucial challenge in this field. Compared to symmetric bulk membranes, fabrication issues can emerge when processing the more complex asymmetric architectures. It is well-known, how shrinkage during thermal treatments of ceramic manufacturers depends, among all the involved parameters, on the composition of the green ceramic body, on the ceramic particles packing and finally, on materials physical-chemical properties. Therefore, combining a gas-tight and thin dense layer with a porous, thick support may lead to a defective sintered membrane due to anisotropic shrinkages and warping effects [69], while delamination and cracks may occur if the two layers are thermo-mechanically incompatible.

To fully exploit ceramic membranes potential, it is therefore paramount to develop efficient and easily-scalable manufacturing processes able to produce highly performant and customized asymmetric ceramic membranes. While in-depth studies on molecular sieves-based systems for gas separation and dense metallic and ceramic membranes can be found elsewhere in the literature [56,70–75], a critical analysis of the production methods to obtain asymmetric architectures of ceramic membranes for hydrogen and oxygen separation has not been published yet. This review will focus on the most used forming techniques and on the new and advanced approaches in the production of ceramic membranes.

2.1. Dual phase membranes

Two different approaches were adopted in the construction of dual-phase systems (Fig. 2), namely mixed- and independently distributed dual-phase membranes. In the first case, which is the most employed, the protonic and electronic conductors are physically mixed in a random design (Fig. 2a). Since the electrochemical transport in these membranes is mainly limited by the electronic conduction, researchers have tried to exploit the external short circuit concept to facilitate the electron transport within the membranes [36], developing independently distributed dual-phase systems in which the two phases are separately distributed (Fig. 2b). These novel architectures allow a reduced diffusion path of the species (i.e., protons/oxygen anions and electrons/holes), and a consequent improvement of the separation performances is thus

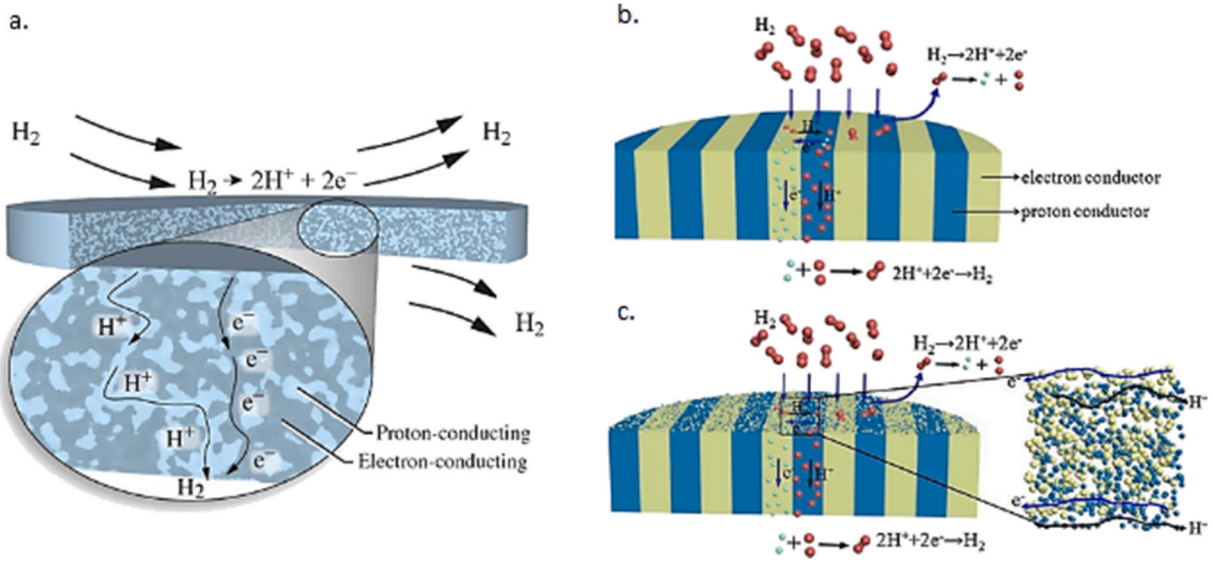

Fig. 2. Schematic representation of (a) a mixed dual-phase ceramic membrane. Reproduced from Ref. [79], (b) an independently distributed dual-phase ceramic membrane [36], (c) surface-modified (mixed powder) independently distributed dual-phase membrane. Reproduced from Ref. [36].

obtained. The transverse resistance of these membranes is increased because of the high transverse diffusion distance of species. It is, therefore, suggested to coat the membrane surface with a mixture of the two phases (Fig. 2c) [36]. However, because of the great technological difficulty associated with the fabrication of this complex architecture, only a few examples have been reported in the literature [76–78].

For a complete overview about the transport mechanisms and material compositions of both hydrogen and oxygen separation membranes, the reader should refer to Refs. [80–82] respectively.

3. Fabrication processes

A variety of different methods have been applied trying to develop easy and scalable membrane fabrication processes able to produce asymmetric configurations with good reproducibility and reliability. Based on the geometry of the membrane, ceramic systems for gas separation have been usually shaped in the form of disks, tubes, and hollow fibers (Fig. 3), where the latter are tubular systems in which the length is much greater than the fiber diameter.

The architecture choice deeply affects both the performances and the fabrication process. Disk membranes (Fig. 3a) are usually the most adopted as they can be easily prepared through simple fabrication processes such as dry-pressing. Their performances are limited by the low surface area and high-temperature sealing [83,84].

On the contrary tubular systems (Fig. 3b), thanks to their higher exchange area, allow the achievement of higher performances. Pressure drops are generally much lower than those typically found in disk-shaped membranes, which constitutes a great operational advantage for industrial plants.

Hollow fiber (Fig. 3c) is a tubular structure with a hollow space inside, with thin walls (*i.e.* 0.1–0.3 mm) and 1–2 mm outer diameters [84]. Considering these dimensions, they possess a large surface area and lengths that are usually much higher than their diameter (*i.e.,* fiber shape). Unlike tubular systems, this structure presents much thinner walls, thus allowing the obtainment of higher performances, as described by the Wagner equation. They can be made with uniformly dense structures, but they are preferably formed as microporous systems, presenting dense selective layers on either the outside surface (sometimes referred to as “shell side”) or on their inside, and with channels distributed along their thickness.

In the following chapters, the most employed fabrication processes will be discussed, for both hydrogen and oxygen separation membranes. To produce asymmetric architectures, more than one ceramic forming processes can be necessary to obtain supports and thin active membranes implying multiple processing steps. This is not always the case for tubular/hollow fibers membranes, which can also be manufactured through one-step fabrication processes (*i.e.,* hollow fiber spinning, double mantle spinning or centrifugal casting, *etc.*) [85,86].

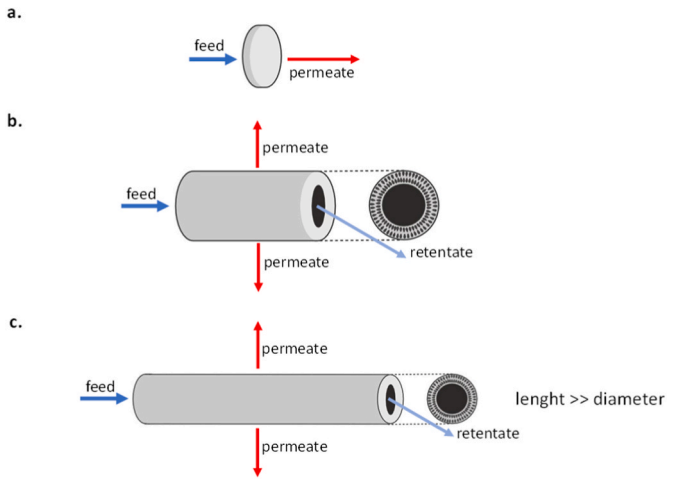

Fig. 3. Schematic representation of a disk (a), tubular (b) and hollow fiber (c) architecture for gas separation membranes.

3.1. Tape casting

Tape casting is a well-known industrially-available technology extensively used in ceramic fabrication to produce both dense and porous substrates and multi-layered materials on a large scale [87]. The standard procedure involves the preparation of a suspension of the inorganic powder, which is dispersed in a liquid, water or organic, with the addition of organic additives such as dispersants, plasticizers and binders. Pore former agents (usually carbon-based materials such as starch, carbon-black, graphite, *etc.*) can be added to the slurry to obtain porous structures upon their combustion during an appropriate thermal treatment [88,89]. The slurry is then cast on top of a moving polymeric substrate through a levelling blade (*i.e.,* the doctor blade) which allows the fine regulation of the thickness of the green tape (Fig. 4). After the drying process, flexible tapes are obtained, which can be cut in the desired shape and laminated onto each other to achieve multilayer green bodies *via* thermo-pressing. The debinding of the organic components and the subsequent sintering step led to the final consolidated ceramic layer/multilayer [90,91].

This technique has been extensively reported in the literature to produce asymmetric membranes, as it is the best way to form large-area, flat ceramics characterized by thin active layers which could not be fabricated by conventional dry-pressing. Coupling this process with a rolling technique also allows the obtainment of tubular membranes.

Recently, phase-inversion tape casting [92], has also been successfully employed to produce oxygen gas separation ceramic membranes. As opposed to the standard procedure, it implies the use of an organic polymer solution-based slurry containing the ceramic powder which, upon contact with a coagulation agent (*i.e.,* a water bath) goes from liquid to a solid state. In the water bath, the organic polymer separates into a polymer-poor phase and a polymer-rich one by exchanging with water. The slurry solidifies into green tapes thanks to the presence of a polymer-rich phase acting as a binder. On the contrary, the polymer-poor phase acts as a pore-forming agent upon its evaporation during a drying step [93,94]. As the phase-inversion process occurs at the polymeric slurry-water interface, asymmetric structures are thus formed, resulting particularly appropriate for gas separation systems. The structure consists of a thick layer with large finger-shaped pores, imparting mechanical strength and low mass-transport resistance, which is coupled to a thin layer possessing adequate features to act as the active separation layer [94].

3.1.1. Hydrogen membranes

Several works have been reported in the literature on dual-phase hydrogen permeation membranes fabricated *via* tape-casting, both for disk and tubular geometries. In 2009 Yoon et al. [95] reported a thin-film tubular hydrogen separation membranes obtained by coating and co-sintering an inner layer of $SrCe_{0.9}Eu_{0.1}O_{3-\delta}$ with a 15 cm long

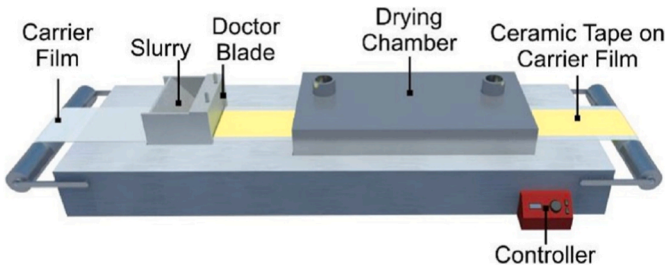

Fig. 4. Schematic representation of a typical tape-casting set-up. Reproduced from Ref. [90].

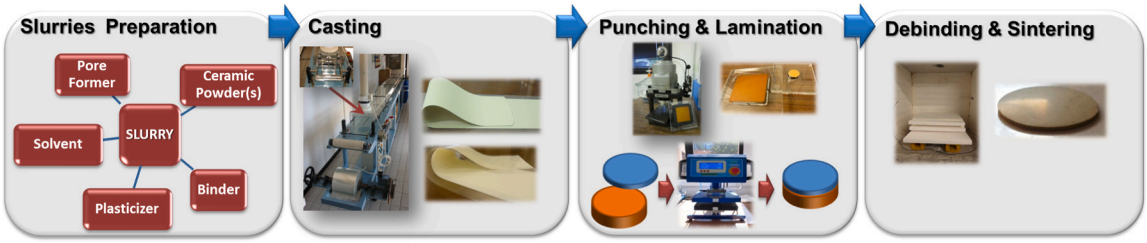

Fig. 5. Schematic representation of the asymmetric $BaCe_{0.65}Zr_{0\cdot20}Y_{0.15}O_{3-\delta}$–$Gd_{0.2}Ce_{0.8}O_{2-\delta}$ (BCZY–GDC) fabrication process. Reproduced from Ref. [100].

tubular support of NiO–$SrCeO_3$ fabricated by rolling a green tape on a circular rod. Upon reduction of NiO to metallic Ni, a certain grade of porosity was achieved in the support obtaining a permeation flux of 2.2 mL min^{-1} at 900 °C, feeding 20 mL min^{-1} of gas composed of 25 % H_2, 3 % H_2O, and balanced Ar.

Some years later, Li et al. [96] proposed an in-depth study on a similar membrane based on $SrCe_{0.7}Zr_{0.2}Eu_{0.1}O_{3-\delta}$ MIEC as active phase, which employed a tape-cast NiO–$SrCe_{0.8}Zr_{0.2}O_{3-\delta}$ tubular support. The influence of the process parameters (*i.e.,* temperature, H_2O and H_2 feed partial pressure, and feed flow rate) on the membrane performance was investigated obtaining a permeation flux of 0.23 mL cm^{-2} min^{-1} at 900 °C in a pure H_2 feed (0.21 mL cm^{-2} min^{-1} in 97 % H_2/3 % H_2O feed). This performance was further improved (0.35 mL cm^{-2} min^{-1} (900 °C, 100 % H_2 feed) by reducing the membrane dense layer thickness from 33 to 17 μm [97].

A multi-layered disk-shaped membrane constituted by a dense layer of $Sr(Ce_{0.6}Zr_{0.4})_{0.85}Y_{0.15}$ $O_{3-\delta}$ (SCZY) and 10 layers of NiO-SCZY (NiO as porous agent upon reduction) as a support substrate was fabricated by Hung et al. [98] through tape casting and lamination of the different layers. This membrane reached a hydrogen permeation flux of 0.184 mmol cm^{-2} min^{-1} at 800 °C in a pure hydrogen feed.

Tape casting and thermo-pressing (Fig. 5) were successfully employed [99,100]to produce a planar dual-phase membrane of $BaCe_{0.65}Zr_{0\cdot20}Y_{0.15}O_{3-\delta}$–$Gd_{0.2}Ce_{0.8}O_{2-\delta}$ (BCZY–GDC) with asymmetrical architecture which displayed superior hydrogen permeation.

In their works [87,99–104] the authors investigate the role of the co-firing process, sintering aid, and atmosphere. The optimization of the fabrication process allowed to obtain asymmetric membranes constituted by a dense 20 μm-thick layer supported by a 750 μm-thick porous layer which showed a hydrogen flux among the highest reported in the literature for all-ceramic membranes of 0.68 mL min^{-1} cm^{-2} at 750 °C for the Pt-activated membrane (feed: 50 % H_2/He, pH_2O = 0.025 atm, sweep: Ar/pH_2O = 0.025 atm).

A regular and independent transport channels-based dual-phase hydrogen membrane (*i.e.,* independently distributed dual-phase system) made of alternating films of $SrCe_{0.9}Y_{0.1}O_{3-\delta}$-$Ce_{0.8}Sm_{0.2}O_2$ (SCY-SDC) has been obtained by cutting along the cross-section a multilayer system produced *via* a combination of tape-casting and co-pressing (Fig. 6) by Meng et al. [76]. In this way, a hydrogen flux of 0.163 mL min^{-1} cm^{-2} (900 °C, feed: 20 % H_2/He, sweep: N_2) was achieved which was much higher compared to the one obtained by a conventional SCY-SDC system. This can be attributed to the shorter diffusion paths for protons and electrons and to the lower amount of phase interfaces created by this membrane architecture. These independently distributed systems possess very interestingly performance, but the permeation benefit in respect to the process effort-cost for their production should be accurately evaluated.

Regarding single-phase membranes, tape-cast hydrogen separation systems have been successfully fabricated over the years, although the examples available are limited to lanthanum tungstate. From the process point of view, single systems present the intrinsic advantage of dealing with only one compound avoiding all the issues related to physical-chemical properties mismatch between phases proper of dual-phase systems (*i.e.,* thermal-expansion coefficient, thermal-stability, sinterability, *etc.*). A $La_6WO_{12-\delta}$ asymmetric membrane was fabricated by Weirich et al. [105]; Deibert et al. [69] reported a preliminary study on an asymmetric $La_{5.4}WO_{12-\delta}$ (LaWO) membrane with an optimized microstructure for hydrogen separation. More recently, a LaWO asymmetric membrane fabricated by tape-casting which reached a hydrogen flux of 0.4 mL min^{-1} cm^{-2} (825 °C in 50 vol% H_2 in He dry feed and humid Ar sweep configuration) [106]. In this case, the application of phase inversion tape casting can be interesting for the performance improvement of asymmetric systems.

A comprehensive overview of the performances achieved by tape-cast ceramic membranes for hydrogen separation is shown in Table 1.

3.1.2. Oxygen membranes

For oxygen separation systems both conventional and inverse phase tape casting techniques have been successfully applied over the years, with a higher number of published works if compared to hydrogen systems.

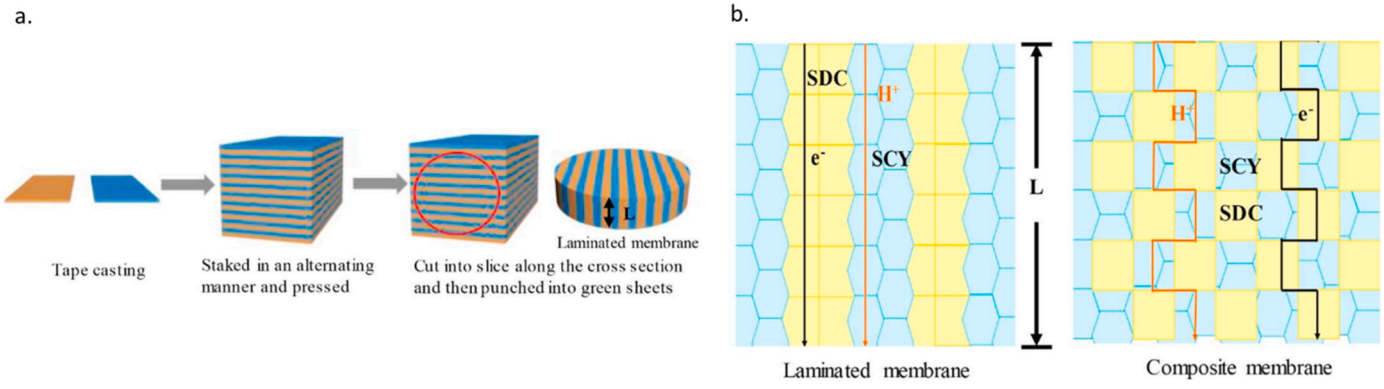

Fig. 6. Schematic illustration of the preparation procedure for dual-phase SCY-SDC laminated membrane with independent transport channels (a) and representation of the transport mechanism of electrons and protons within the membrane compared to a classical composite system (b). Reproduced from Ref. [76].

Table 1
Tape-casted hydrogen and oxygen permeation ceramic membranes performances reported in the literature. Bold systems indicate active (dense) layers whereas italic is used for supports.

Tape Casting								
Hydrogen separation membranes								
System	Architecture	Configuration	Tape cast part	Thickness [mm]	J [mL cm^{-2} min^{-1}]	Feed/ Sweep gasses	T [°C]	Ref.
$SrCe_{0.9}Eu_{0.1}O_{3-\delta}$ *–NiO–$SrCeO_3$*	tubular	Single-phase - asymmetric	support (dense layer via colloidal coating)	0.030 (dense layer)	2.2 mL min^{-1}	25 % H_2 -Ar-3% H_2O/He	900	[95]
$SrCe_{0.7}Zr_{0.2}Eu_{0.1}O_{3-\delta}$ – *NiO–$SrCe_{0.8}Zr_{0.2}O_{3-\delta}$*	tubular	Single-phase – asymmetric	support (dense layer via colloidal coating)	0.033 (dense layer)	0.23	100 % H_2	900	[96]
$SrCe_{0.7}Zr_{0.2}Eu_{0.1}O_{3-\delta}$ – *NiO–$SrCe_{0.8}Zr_{0.2}O_{3-\delta}$*	tubular	Single-phase – asymmetric	support (dense layer via slurry coating)	0.017 (dense layer)	0.35	100 % H_2	900	[97]
$Sr(Ce_{0.6}Zr_{0.4})_{0.85}Y_{0.15}$ $O_{3-\delta}$ (SCZY)– *SCZY-NiO*	disk	Single-phase – asymmetric	dense - support	0.017 (dense layer)	0.184 mmol cm^{-2} min^{-1}	100 % H_2	800	[98]
$BaCe_{0.65}Zr_{0.20}Y_{0.15}O_{3-\delta}$ (BCZY)– $Gd_{0.2}Ce_{0.8}O_{2-\delta}$ (GDC) - *(BCZY -GDC)*	disk	Dual-phase – asymmetric	dense - support	0.020 (dense layer)	0.68	Wet H_2–He/ Ar–H_2O	750	[99]
$SrCe_{0.9}Y_{0.1}$ $O_{3-\delta}$ -$Ce_{0.8}Sm_{0.2}O_2$ (SCY-SDC)	disk	Dual-phase independently distributed - symmetric	dense (whole membrane)	1 (whole membrane)	0.163	20 % H_2 -He/N_2	900	[76]
$La_{28-x}W_{4+x}O_{54+\delta}$ (LaWO) – *LaWO*	disk	Single phase - asymmetric	dense -support	0.030 (dense layer)	0.4	50 % H_2 -He/Air- H_2O	825	[106]
Oxygen separation membranes								
$CaTi_{0.9}Fe_{0.1}$ $O_{3-\delta}$ (CTF) – *CTF*	disk	Single-phase - asymmetric	dense -support	0.030 (dense layer)	0.45	Air/Ar	1000	[107]
$Ba_{0.5}Sr_{0.5}Co_{0.8}Fe_{0.2}O_{3-\delta}$ (BSFC) – *BSFC*	disk	Single-phase - asymmetric	dense -support	0.070 (dense layer)	67.7	O_2/Ar	1000	[108]
$La_{0.6}Sr_{0.4}Co_{0.2}Fe_{0.8}O_{3-\delta}$ (LSCF) – *LSCF*	disk	Single-phase - asymmetric	dense -support	0.030 (dense layer)	13.3	O_2/Ar	1000	[109]
$La_{0.58}Sr_{0.4}Co_{0.2}Fe_{0.8}O_{3-\delta}$ (LSCF) – *LSCF*	disk	Single-phase - asymmetric	dense -support	0.030 (dense layer)	1	Air/Ar	850	[110]
$La_{0.6}Sr_{0.4}Co_{0.2}Fe_{0.8}O_{3-\delta}$ (LSCF) – *LSCF*	disk	Single-phase - asymmetric	dense -support	0.020 (dense layer)	1.2	Air/Ar	900	[111]
$(La_{0.6}Ca_{0.4})_{0.98}$ $(Co_{0.8}Fe_{0.2})O_{3-\delta}$ (LCCF) – *LCCF*	disk	Single-phase - asymmetric	dense -support	0.025 (dense layer)	3.32	O_2/N_2	900	[112]
$La_{0.7}Sr_{0.3}MnO_3$ – $Gd_{0.1}Ce_{0.9}O_{2-\delta}$	disk	Dual-phase - independently distributed	dense (whole membrane)	0.100 (whole membrane)	1.31	Air/He	850	[77]
$La_{0.7}Sr_{0.3}MnO_3$ – $(ZrO_2)_{0.92}(Y_2O_3)_{0.08}$ (8YSZ)	disk	Dual-phase - independently distributed	dense (whole membrane)	0.100 (whole membrane)	0.1	Air/He	800	[78]
$Ce_{0.85}Sm_{0.15}O_{2-\delta}$ (SDC) – $Sm_{0.6}Sr_{0.4}Al_{0.3}Fe_{0.7}O_{3-\delta}$ (SSAF) – *(SDC-SSAF)*	disk	Dual-phase – asymmetric	dense -support	0.040	3.9	Air/He	950	[113]
$(Y_2O_3)_{0.01}(Sc_2O_3)_{0.10}(ZrO_2)_{0.89}$ (10Sc1YSZ)- $MnCo_2O_4$ – (*3YSZ/ Al_2O_3*)	disk	Dual-phase – asymmetric	dense -support	0.007	2.3	O_2/N_2	940	[114]

3.1.2.1. Conventional tape casting. Tape-casting coupled with co-lamination, and co-sintering of the green tapes, has been applied to produce asymmetric ceramic systems for oxygen permeation. Single-phase membranes have been reported with the process advantages already discussed. $CaTi_{0.9}Fe_{0.1}O_{3-\delta}$ [107], $Ba_{0.5}Sr_{0.5}Co_{0.8}Fe_{0.2}O_{3-\delta}$ [108], $La_{0.6}Sr_{0.4}Co_{0.2}Fe_{0.8}O_{3-\delta}$ [109–111], $(La_{0.6}Ca_{0.4})_{0.98}$ $(Co_{0.8}Fe_{0.2})$ $O_{3-\delta}$ [112] membranes are reported in the literature; their performances are summarised in Table 1.

An independently distributed dense membrane produced by tape-casting has been fabricated by alternating electron conducting segments of LSM ($La_{0.7}Sr_{0.3}MnO_3$) with GDC ($Ce_{0.9}Gd0.1O_{2-\delta}$) blocks [77]. The optimized system (three GDC blocks, two LSM segments) achieved an oxygen flux of 1.31 mL min^{-1} cm^{-2} at 850 °C (feed: dry air, sweep: He). A similar segmented structure was proposed by the same authors [78] to produce an LSM ($La_{0.7}Sr_{0.3}MnO_{3\pm\delta}$) – 8YSZ ($(ZrO_2)_{0.92}(Y_2O_3)_{0.08}$) dual phase membrane, with the aim of solving the problem of reactivity encountered during high-temperature sintering of these two phases. A disk-shaped dense membrane consisting of a central 100 μm-thick LSM segment between two lateral YSZ layers was therefore fabricated for this purpose (Fig. 7). A permeation flux of an order of magnitude higher than the one of a conventional dual-phase dense membrane of the same components was registered (0.1 mL cm^{-2} min^{-1}, 800 °C, dry air/He as the feed/sweep respectively), demonstrating the possibility to employ this novel architecture to overcome the conventional limitations of composite membranes.

Asymmetric dual-phase $Ce_{0.85}Sm_{0.15}O_{2-\delta}$ – $Sm_{0.6}Sr_{0.4}Al_{0.3}Fe_{0.7}O_{3-\delta}$ -based system was proposed by Cao et al. [113] that achieved a 3.9 mL min^{-1} cm^{-2} O_2 flux at 950 °C when dry air and helium were fed to the porous support side and permeate side respectively.

A multi-layered asymmetric membrane consisting of a $(Y_2O_3)_{0.01}(Sc_2O_3)_{0.10}(ZrO_2)_{0.89}$ (10Sc1YSZ)- $MnCo_2O_4$ thin dense layer sandwiched between two porous 8YSZ layers and supported by a 3YSZ/ Al_2O_3 substrate was reported [114], with an oxygen flux of 2.3 mL min^{-1} cm^{-2} at 940 °C in a pure oxygen feed (N_2 as sweep gas).

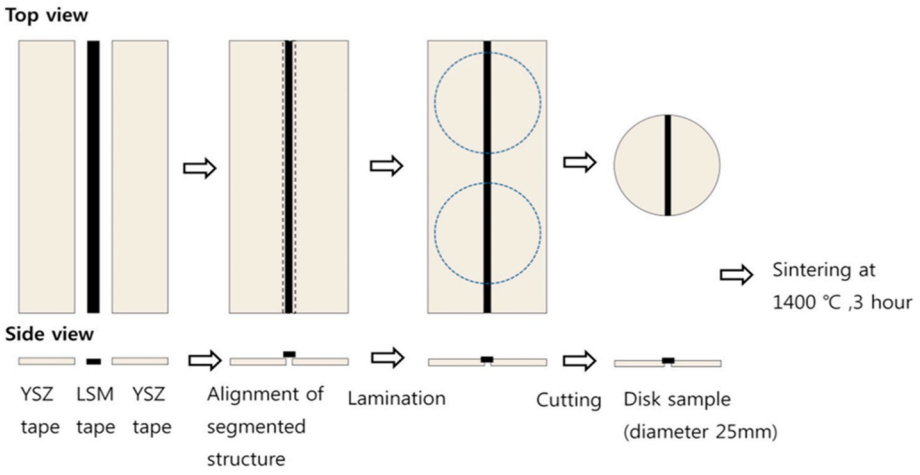

Fig. 7. The top and side view of schematic drawings of the lamination and cutting processes for the segmented LSM-YSZ tape-cast oxygen membrane. Reproduced from Ref. [78].

3.1.2.2. Phase inversion tape casting. This process has been employed for the fabrication of oxygen transport membranes due to the possibility of obtaining, in a one-step process, dense-porous asymmetric structures characterized by a directional porosity of the porous substrate (Table 2). A single-phase asymmetric $La_{0.6}Sr_{0.4}Co_{0.2}Fe_{0.8}O_{3-\delta}$ (LSCF) membrane has been prepared by Meng et al. [115] by coupling a porous support fabricated by phase-inversion tape-casting, with a dense thin LSCF layer (~40 μm thick) fabricated *via* conventional tape-casting. A screen-printed thin catalytic layer of porous LSCF was also deposited and the final membrane achieved a 1.54 mL cm^{-2} min^{-1} oxygen flux in air/He gradient at 900 °C. This result was 2.5 times higher than that of a similar membrane prepared by conventional tape casting used as a reference.

Dual-phase membranes made of a 1:1 mixture of $Zr_{0.84}Y_{0.16}O_{1.92}$ -$La_{0.8}Sr_{0.2}MnO_{3-\delta}$ were prepared by a one-step phase inversion tape casting process by He et al. [94]. The asymmetric two-layered structure consisting of a thick porous support and a relatively thin gastight layer (oxygen separation function) showed a significantly higher oxygen permeability of 1.90×10^{-3} mol m^{-2} s^{-1} compared to the 3.31×10^{-4} mol m^{-2} s^{-1} one achieved by a membrane prepared by a two-step conventional tape casting in the same operational conditions (*i.e.,* 900 °C, Air/He as feed/sweep). Huang et al. [116] prepared a $Ce_{0.9}Gd_{0.1}O_{1.95}$–$La_{0.6}Sr_{0.4}Co_{0.2}Fe_{0.8}O_{3-\delta}$ asymmetric membrane *via* phase inversion tape casting on top of which an activation layer of porous $La_{0.6}Sr_{0.4}CoO_{3-\delta}$ was deposited. The oxygen permeation flux was improved by a factor of 4.1–5.6, reaching an O_2 permeation of 0.45 mL cm^{-2} min^{-1} at 900 °C (Air/He as feed/sweep).

Phase inversion tape casting was also employed by Zhang et al. to produce planar composite of $Zr_{0.84}Y_{0.16}O_{1.92}$–$La_{0.8}Sr_{0.2}Cr_{0.5}Fe_{0.5}O_{3-\delta}$ (YSZ-LSCrF) [117]. The dual-phase membrane (25 μm thick dense layer) was modified with a porous screen-printed activation layer (dense side) of YSZ-LSCrF (60:40 vol ratio) and impregnated with $Sm_{0.2}Ce_{0.8}O_{2-\delta}$ (SDC) registering an oxygen permeation flux of 2.1 mL cm^{-2} min^{-1} (850 °C, Air/CO as feed/sweep) [118]. The proposed process was then optimized using two distinct slurries for the dense layer and the porous support respectively, achieving an improved oxygen flux of 2.4 mL cm^{-2} min^{-1} under the same condition [117].

A one-step phase-inversion tape-casting was also reported for asymmetric $Gd_{0.1}Ce_{0.9}O_{1.95-\delta}$–$La_{0.6}Sr_{0.4}FeO_{3-\delta}$ [119]. The membrane, properly modified by depositing a porous screen-printed catalytic layer (permeate side), registered an oxygen permeation flux of 1.49 mL cm^{-2} min^{-1} at 900 °C (Air/He as feed/sweep).

A new variant of phase inversion tape casting was employed by Yuan et al. [120] to fabricate a dual-phase planar membrane made of

Table 2
Oxygen permeation ceramic membrane and relative performances for the phase inversion tape-cast systems reported in the literature. Bold systems indicate active (dense) layers whereas italic is used for supports.

Phase Inversion Tape Casting								
Oxygen separation membranes								
System	Architecture	Configuration	Tape cast part	Thickness [mm]	J [mL cm^{-2} min^{-1}]	Feed/ Sweep gasses	T [°C]	Ref.
$La_{0.6}Sr_{0.4}Co_{0.2}Fe_{0.8}O_{3-\delta}$ (LSCF) – *LSCF*	disk	Single-phase - asymmetric	support	0.040 (dense layer)	1.54	Air/He	900	[115]
$Zr_{0.84}Y_{0.16}O_{1.92}$ (YSZ) -$La_{0.8}Sr_{0.2}MnO_{3-\delta}$ (LSMO) – *(YSZ-LSMO)*	disk	Dual-phase -asymmetric	dense-support	0.15 (dense layer)	1.90×10^{-3} [mol m^{-2} s^{-1}]	Air/He	900	[94]
$Ce_{0.9}Gd_{0.1}O_{1.95}$ (GDC)–$La_{0.6}Sr_{0.4}Co_{0.2}Fe_{0.8}O_{3-\delta}$ (LSCF) – *(GDC-LSCF)*	disk	Dual-phase -asymmetric	dense-support	0.100 (dense layer)	0.45	Air/He	900	[116]
$Zr_{0.84}Y_{0.16}O_{1.92}$–$La_{0.8}Sr_{0.2}Cr_{0.5}Fe_{0.5}O_{3-\delta}$ (YSZ-LSCrF) – *(YSZ-LSCrF)*	disk	Dual-phase -asymmetric	dense-support	0.030 (dense layer)	2.4	Air/CO	900	[117]
$Zr_{0.84}Y_{0.16}O_{1.92}$–$La_{0.8}Sr_{0.2}Cr_{0.5}Fe_{0.5}O_{3-\delta}$ (YSZ-LSCrF) – *(YSZ-LSCrF)*	disk	Dual-phase -asymmetric	dense-support	0.025 (dense layer)	2.1	Air/CO	850	[118]
$Gd_{0.1}Ce_{0.9}O_{1.95-\delta}$ (GDC)—$La_{0.6}Sr_{0.4}FeO_{3-\delta}$ (LSF) – *(GDC-LSF)*	disk	Dual-phase -asymmetric	dense-support	0.100 (dense layer)	1.49	Air/He	900	[41]
$Zr_{0.84}Y_{0.16}O_{1.92}$–$La_{0.8}Sr_{0.2}Cr_{0.5}Fe_{0.5}O_{3-\delta}$ (YSZ–LSCrF) – *(YSZ-LSCrF)*	disk	Dual-phase -asymmetric	dense-support	0.150 (dense layer)	1	Air/CO	850	[120]
$Zr_{0.84}Y_{0.16}O_{1.92}$–$La_{0.8}Sr_{0.2}Cr_{0.5}Fe_{0.5}O_{3-\delta}$ (YSZ–LSCrF) – *(YSZ-LSCrF)*	disk	Dual-phase -symmetric	dense-support	0.005 (dense layer)	1.95	Air/CO	900	[121]

$Zr_{0.84}Y_{0.16}O_{1.92}$–$La_{0.8}Sr_{0.2}Cr_{0.5}Fe_{0.5}O_{3-\delta}$ (YSZ–LSCrF) with a fully opened oriented porosity thanks to the use of a graphitic thin layer. A slurry containing the two oxide powders was co-tape cast with a slurry of graphite (skin-layer) and successively solidified in a green tape by immersion in water. In this way, a novel three-layered structure made of a relatively dense layer deriving from the graphite slurry, on top of a characteristic finger-like porous layer in the middle and a sponge-like layer at the bottom (both deriving from the YSZ–LSCrF slurry) was obtained in the green tape. The finger-like porous section of about 850 μm, with fully opened finger-like pores, was responsible for the fast mass transport (Fig. 8 a,b). A membrane prepared by conventional phase inversion tape casting was also fabricated for comparison, showing a blocked support porosity because of the presence of a low porous top layer at the outermost area of the support (*i.e.,* feed side), where the graphitic layer was not applied. The optimized system modified with nano-SDC (porous side) and a porous screen-printed YSZ-LSCrF layer (dense side) achieved an oxygen flux of 1 mL cm^{-2} min^{-1} at 850 °C (Air/CO as feed/sweep).

Recently, this two-slurry graphite-based process was employed to fabricate an innovative sandwich-like symmetric dual-phase membrane with an ultrathin oxygen separation layer by Li et *al.* [121]. The membrane consisted of a 5 μm thick dense oxygen separation layer sandwiched between two 300 μm thick finger-like porous layers (Fig. 9). This innovative structure was achieved by lamination and pressing of two distinct green tapes along their dense side obtained by phase-inversion tape casting with graphitic skin layers. The as-obtained membrane was modified with $Sm_{0.2}Ce_{0.8}O_{2-\delta}$ nanoparticles to promote the surface oxygen exchange achieving a permeation flux of 1.95 mL cm^{-2} min^{-1} at 900 °C (Air/CO as feed/sweep). The research in this field gives a clear indication that the exploiting of finger-like structures and the addition of nanometric particles can improve the oxygen flux of the produced systems. More works in this direction can, therefore, help the technology transfer and application in the industrial field.

3.2. Freeze casting

In the fabrication of performant asymmetric ceramic gas-separation membranes, the substrate microstructure plays a fundamental role in increasing the gas diffusivity through the porous support thus influencing the overall separation performance. The final goal is to decrease the mass transfer resistance to allow the operation at high flow streams, with beneficial advantages for industrial application [122]. In this perspective, freeze casting represents an interesting technique for the preparation of highly oriented porous supports with low tortuosity. In this method, a ceramic slurry is prepared, poured into a mold, placed onto a freezing substrate, and directionally frozen. The removal of the frozen dispersing medium (*i.e.* the solvent) by sublimation leaves pores in the ceramic green body which are preserved after sintering (Fig. 10) [123–126]. Hydrogen and oxygen separation systems produced by freeze casting were summarized in Table 3.

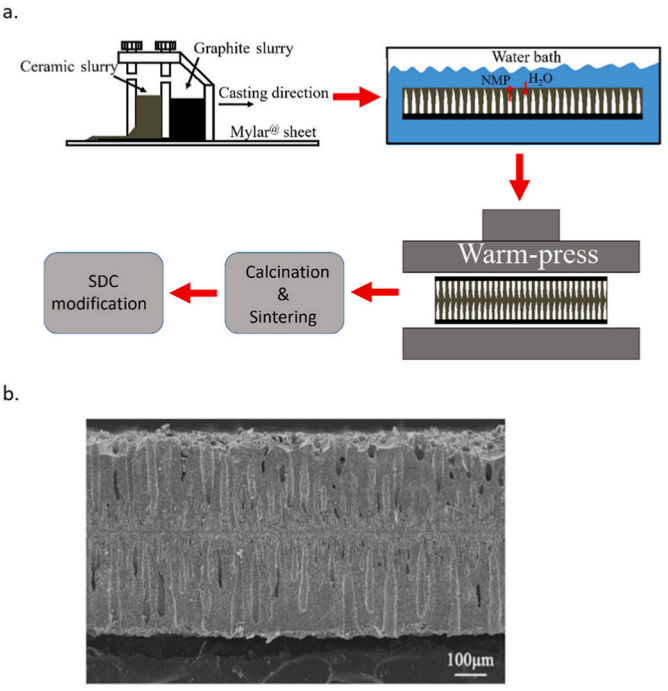

Fig. 9. Schematic representation of the phase inversion process and warm-pressing employed to produce the $Zr_{0.84}Y_{0.16}O_{1.92}$ – $La_{0.8}Sr_{0.2}Cr_{0.5}Fe_{0.5}O_{3-\delta}$ membrane (a), and SEM image of the final product (b). NMP: N-Methyl pyrrolidone Modified from Ref. [121].

3.2.1. Hydrogen membranes

The only available example of freeze casting applied to hydrogen separation technology has been recently reported [122]. In this work, ice-templating was applied to $BaCe_{0.65}Zr_{0.20}Y_{0.15}O_{3-\delta}$–$Gd_{0.2}Ce_{0.8}O_{2-\delta}$ (BCZY–GDC) to fabricate a dual phase membrane support with aligned porosity (Fig. 11). A BCZY-GDC support with good mechanical properties and N_2 permeability of one order of magnitude higher compared to the ones achieved by tape cast BCZY-GDC substrates was fabricated. A screen printed BCZY-GDC active layer was successfully deposited on the freeze cast substrate obtaining hierarchically structured membranes showing promising H_2 fluxes of 0.36 and 0.42 mL min^{-1} cm^{-2} at 750 °C, using a feed stream with 50 and 80 % H_2 in He respectively [127].

3.2.2. Oxygen membranes

Freeze casting is more frequently used for oxygen separation systems. Gaudillere et al. [128] fabricated an asymmetric dual-phase oxygen permeation membrane by combining a freeze cast $La_{0.6}Sr_{0.4}Co_{0.2}Fe_{0.8}O_{3-\delta}$ (LSCF) support with hierarchically oriented porosity and a screen-printed dense and gas-tight functional layer of $NiFe_2O_4$/$Ce_{0.8}Tb_{0.2}O_{2-\delta}$ (NFO/CTO) on top. This multi-layered system was composed of a porous LSCF support and a fully densified layer of

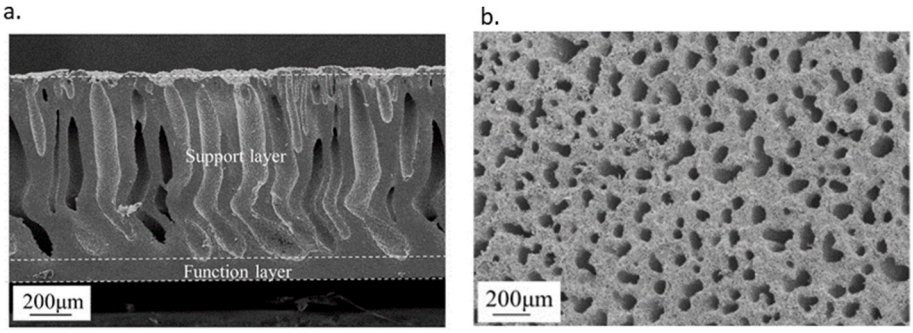

Fig. 8. SEM image of the cross-section of the membrane (a); SEM image of the surface of the support layer showing the open porosity (b). Modified from Ref. [120].

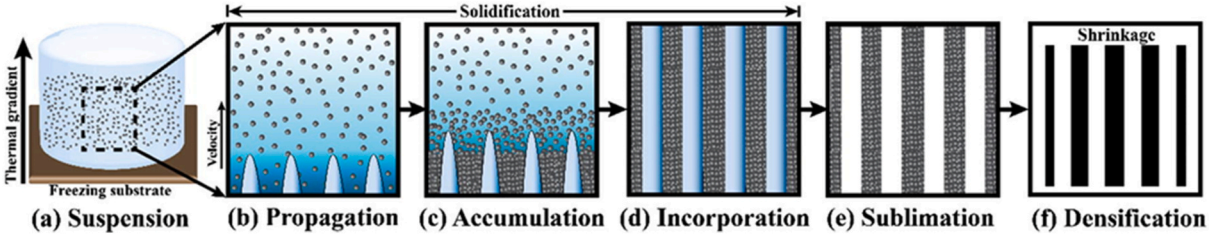

Fig. 10. Schematic representation of the different steps of the freeze-casting process. Reproduced from Ref. [126].

Table 3
Hydrogen and oxygen permeation ceramic membranes and relative performances (if available) for the freeze casting systems reported in the literature. Bold systems indicate active (dense) layers whereas italic is used for supports.

Freeze Casting								
Hydrogen separation membranes								
System	Architecture	Configuration	Freeze cast part	Thickness [mm]	J [mL cm^{-2} min^{-1}]	Feed/ Sweep gasses	T [°C]	Ref.
$BaCe_{0.65}Zr_{0.20}Y_{0.15}O_{3-\delta}$ (BCZY)–$Gd_{0.2}Ce_{0.8}O_{2-\delta}$ (GDC)	disk	Dual-phase – asymmetric	membrane	0.85 (support) 0.013 (dense layer)	0.36	50 % H_2 in He/Ar	750	[122, 127]
Oxygen separation membranes								
$NiFe_2O_4$ (NFO)–$Ce_{0.8}Tb_{0.2}O_{2-\delta}$ (CTO) – *$La_{0.6}Sr_{0.4}Co_{0.2}Fe_{0.8}O_{3-\delta}$ (LSCF)-*	disk	Dual-phase -asymmetric	support (dense layer via screen printing)	0.018 (dense layer)	12	O_2/Ar	1000	[128]
$La_{0.6}Sr_{0.4}Co_{0.2}Fe_{0.8}O_{3-\delta}$ (LSCF)-*LSCF*	disk	Single-phase -asymmetric	support (dense layer via screen printing)	0.030 (dense layer)	6.8	Air/Ar	1000	[129]
***3YSZ** (3 % mol Y_2O_3 doped ZrO_2)*	disk	Single-phase - support	support	–	–	–	–	[130]
$Ba_{0.5}Sr_{0.5}Co_{0.8}Fe_{0.2}O_{3-\delta}$ (BSCF) – *BSCF*	disk	Single-phase- asymmetric	support (dense layer via dip-coating)	0.020 (dense layer)	–	–	–	[132]
$La_{0.8}Sr_{0.2}Cr_{0.5}Fe_{0.5}O_{3-\delta}$ (LSCFO) – *$Ce_{0.8}Gd_{0.15}Co_{0.05}O_{2-\delta}$ (GDC-Co as interlayer) $(ZrO_2)_{0.97}(Y_2O_3)_{0.03}$ (3YSZ)*	tubular	Single-phase -asymmetric	support (dense and interlayer via dip-coating)	0.030 (dense layer)	0.31	Air/Ar	1000	[134]

LSCF (10 μm thick) on top of it, both formed during the freeze-casting step. The active dense layer (8 μm thick) of NFO/CTO was then applied by screen printing. The oxygen permeation registered was 4.8 mL cm^{-2} min^{-1} at 1000 °C (air/Ar as feed/sweep) which increased up to 12 mL cm^{-2} min^{-1} when pure oxygen was fed. This demonstrated the great potential of this technique to obtain asymmetric membranes with an optimal porosity, together with a gas-tight functional layer in a one-step.

The promising results achievable fabricating *via* freeze casting a single-phase oxygen membrane comprised of a porous $La_{0.6}Sr_{0.4}Co_{0.2}Fe_{0.8}O_{3-\delta}$ support covered with a screen-printed dense layer (30 μm thick) of the same material were also shown [129]. The permeation flux of 6.8 mL cm^{-2} min^{-1} (1000 °C, Air/Ar feed/sweep) was markedly above the results registered for LSCF membranes prepared by conventional technique, and still remain among the highest reported in the literature.

Supports produced by freeze casting usually display much lower pressure drops at the expense of a generally inferior mechanical stability. A study conducted by Zou et al. [130] on 3 % molar Y_2O_3 doped ZrO_2 (3YSZ) investigated the influence of the degree of porosity and pore structure on the mechanical properties (*i.e.* elastic modulus and fracture stress) and flow resistance of freeze cast supports. Lower elastic modulus and fracture strength were registered for freeze cast samples; however, the rather high critical strain indicated a potentially even superior behaviour for the freeze cast supports under the action of thermally induced strains (*i.e.,* the difference in thermal expansion). There was no monotonous decrement in the mechanical strength with the increase in porosity. The mechanical resistance of freeze cast specimen depends, in fact, not only on the overall porosity but is also strictly related to the pore structure and size. Therefore, as stressed by the authors, an optimized balance between flow resistance and mechanical strength needs to be achieved, which is not always easy to predict for the numerous parameters involved.

As proof of the complexity of these systems, an unexpected outcome was achieved by Schulze-Küppers et al. [131]. They conducted an in-depth comparison between freeze and tape casting for the fabrication of porous $Ba_{0.5}Sr_{0.5}(Co_{0.8}Fe_{0.2})_{0.97}Zr_{0.03}O_{3-\delta}$ with the aim of identifying the relevant microstructural parameters involved in the superior permeation of freeze cast support. In the study, the oxygen fluxes of asymmetric systems consisting of a surface-activated 20 μm thick membrane layer with tape- or freeze-cast supports identical in pore volumes and layers thickness were measured, showing no improvement when the freeze-cast support was employed. The explanation for this unconventional result was attributed to the constrain diffusivity in freeze cast samples due to the insufficient porosity and pore opening diameters within the nucleation and transition zones of the freeze-cast sample (*i.e.,* the region between the porous and dense layer). Although the result was achieved with a non-optimized freeze cast support, as stated by the authors, this work is an example of the many aspects that must be considered when producing a performant freeze cast support for permeation gas membrane, which can make the design of these systems not always straightforward.

A coupled process between freeze-casting and dip-coating was reported in the literature by Souza et al. [132] for $Ba_{0.5}Sr_{0.5}Co_{0.8}Fe_{0.2}O_{3-\delta}$ (BSCF) membranes. A dense active BSCF layer of about 20 μm thick, free of cracks, was fabricated on top of the freeze cast support. No delamination between the dense dip-coated layer and the porous substrate was observed demonstrating the effective possibility of coupling the two

techniques.

Rachadel et al. [133] proposed, with the same purpose, tape-casting as a suitable method to fabricate the thin dense active layer; they produced an asymmetric system based on freeze-cast BSCF support and thin Zr-doped BSCF (BCSFZ) tape-cast active layer without observing any delamination.

Few examples are also reported for the fabrication of tubular membrane supports by freeze-casting. Gaudillere et al. [134] reported an asymmetric tubular membrane made of a freeze cast 3YSZ consisting in a 15 μm-thick hierarchical and radial-oriented porous structure separated by a fully densified wall of about 2 μm. This support was successively dip-coated to get a $Ce_{0.8}Gd_{0.15}Co_{0.05}O_{2-\delta}$ (GDC-Co) interlayer of 8 μm to avoid the well-known chemical interaction between YSZ and the outer 80 μm-thick active dense layer of $La_{0.8}Sr_{0.2}Cr_{0.5}Fe_{0.5}O_{3-\delta}$ (LSCrF). Despite the low oxygen flux (0.31 mL cm^{-2} min^{-1} 1000 °C, Air/Ar as sweep/feed), ascribed to the non-optimal porosity degree of the GDC-Co interlayer, this work demonstrated the possibility to employ this technique for the fabrication of tubular separation membranes.

3.3. Freeze-tape casting

Recently, a new take on the freeze-casting method has been proposed which couples the ice-templating technique with conventional tape-casting. This procedure consists in casting a liquid (water/solvent-based) slurry of the ceramic powder onto a planar substrate and subsequently subjecting the as-obtained cast system to directional freezing. Two steps of sublimation and sintering, as for a standard freeze-casting method, then follow. In this way, large tapes with a directional microstructured porosity perpendicular to the casting direction can be obtained. The clear advantage of this version is the complete control of the thickness of the deposited sample, as opposed to the conventional freeze-casting, directly given by the gap of the blades used in the process.

An example reported for oxygen separation systems is attributable to Liu et al. [135] who applied this innovative forming procedure to the production of asymmetric $Ce_{0.9}Gd_{0.1}O_{1.95}$-$(La_{0.8}Sr_{0.2})_{0.95}MnO_{3-\delta}$ (GDC-LSM) membrane. A freeze-tape cast support (870 μm thick) with gradient straight pores with low tortuosity factor was fabricated, promoting fast gas diffusion in the membrane. On its top, a dense GDC-LSM film (30 μm thick) and a $Ce_{0.8}Sm_{0.2}O_{1.9}$ (SDC)-$La_{0.6}Sr_{0.4}Co_{0.2}Fe_{0.8}O_{3-\delta}$ (LSCF) surface modification layer (20 μm thick) were screen-printed onto the disk-shaped pre-sintered support and co-sintered to obtain the final membrane. The obtained system registered an 1100 % higher oxygen permeation flux of 0.758 mL cm^{-2} min^{-1} (950 °C, Air/He as feed/sweep) compared to the corresponding symmetric membrane with the same thickness obtained by conventional methods (*i.e.* dry-pressing, see *paragraph 4.5*).

The same authors applied this procedure to the fabrication of a dual-phase $Zr_{0.84}Y_{0.16}O_{1.92}$-$La_{0.8}Sr_{0.2}Cr_{0.5}Fe_{0.5}O_{3-\delta}$ asymmetric membrane. The as-obtained membrane was made of a hierarchically structured porous support and a thin dense layer (~20 μm thick) displaying an enhanced oxygen permeation flux of 2.23 mL cm^{-2} min^{-1} (950 °C, Air/CO as feed/sweep) [136] which could be partly attributed to the decreased gas diffusion resistance in the freeze cast support. These results were summarized in Table 4.

3.4. Extrusion

The extrusion relies on the passage of a plastic ceramic body (conventional extrusion) or ceramic slurry (hollow fiber process) through a die orifice under high-pressure conditions. The geometry of the final system is determined by the die dimensions and by the length of the cutting. After shaping, structures are usually consolidated through a sintering process [137].

The success of the conventional extrusion process is strongly dependent on the plasticity of the material to be extruded (the material ability to be deformed without rupture) through the application of a mechanical stress, and to retain the deformation when stress is removed or reduced. The ceramic paste to be extruded is generally formulated considering solvent-based [138] or thermoplastic binder [139] systems; in the first case, a pre-dissolved binder in water or an alcohol-based solvent is added to the ceramic powder, while the latter considers the use of thermoplastic polymers such as polyethylene (PE), polypropylene (PP) or ethylene-vinyl acetate copolymer (EVA) which soften, melt or become more pliable upon heating, and harden during cooling (reversible physical process). Tube-shaped membranes with wall thickness in the 0.8–2.0 mm range are usually obtained with this technique.

A combination of extrusion and phase inversion/gelation techniques

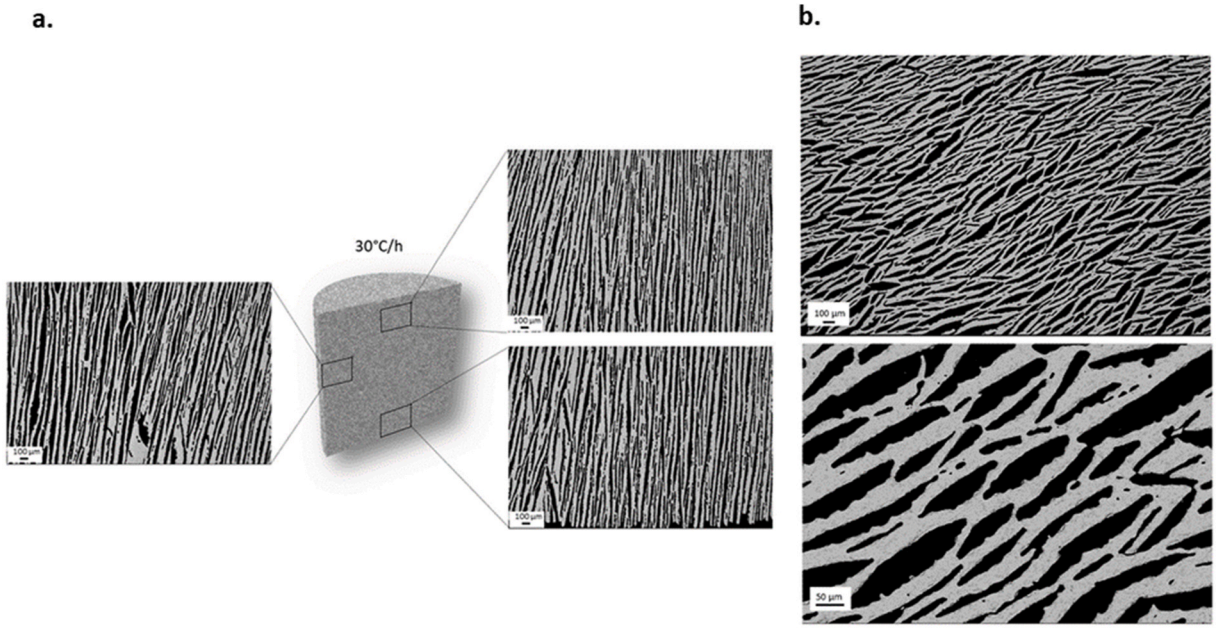

Fig. 11. SEM micrographs of the vertical cross-section, collected in different parts of the sample (a) and (b) horizontal cross-section at different magnitudes for the optimized BCZY-GDC support obtained at a freezing rate of 30 °C/h. Modified from Ref. [122].

Table 4
Oxygen permeation ceramic membranes and relative performances (if available) for the freeze casting systems reported in the literature. Bold systems indicate active (dense) layers whereas italic is used for supports.

Freeze-Tape Casting								
Oxygen separation membranes								
System	Architecture	Configuration	Freeze-tape cast part	Thickness [mm]	J [mL cm^{-2} min^{-1}]	Feed/ Sweep gasses	T [°C]	Ref.
$Ce_{0.9}Gd_{0.1}O_{1.95}$-$(La_{0.8}Sr_{0.2})_{0.95}MnO_{3-\delta}$ (GDC-LSM) – *(GDC-LSM)*	disk	Dual-phase -asymmetric	dense (LSCF) -support	0.030 (dense layer)	0.758	Air/He	950	[135]
$Zr_{0.84}Y_{0.16}O_{1.92}$ (YSZ) -$La_{0.8}Sr_{0.2}Cr_{0.5}Fe_{0.5}O_{3-\delta}$ (LSCFO) – *(YSZ-LSCFO)*	disk	Dual-phase -asymmetric	support (dense layer *via* screen printing)	0.020 (dense layer)	2.23	Air/CO	950	[136]

is, on the other hand, necessary for the fabrication of hollow fibers, leading to wall thicknesses usually in the range of 100–500 μm. This method starts with the preparation of a dope mixture, where the ceramic powders are combined into a solution containing a polymeric binder and solvent. After mixing, the obtained dope suspension is spun into hollow fibers as displayed in Fig. 12 [137]. The dope solution is injected through a spinneret under pressure, while a pressurized liquid (*i.e.,* bore liquid) is injected into the inner shell. In this way, a hollow fiber ceramic piece is formed, which is completed upon contact with a coagulation bath. Binders that deliver the best spinning properties are usually based on sulphur containing polymers such as polyether sulfone (PESF) or polysulfone (PSF) [140].

Extrusion-based techniques have been employed for the fabrication of tubular and hollow fibers membranes, especially for oxygen separation systems. Compared to other techniques, such as, for example, the tape-casting/rolling method, extrusion allows the fabrication of much more mechanically resistant ceramic bodies, permitting a fine control of dimensions, despite the usually relatively thicker walls associated. Hydrogen and oxygen membranes produced using this techique were summarized in Table 5.

3.4.1. Hydrogen membranes

For tubular systems, Gurauskis et al. [141] recently reported the production of asymmetric lanthanum tungstate-based membranes obtained by combining a tubular porous support (EVA as the thermoplastic binder, ~ 7.5 mm diameter and ~0.8 mm thick) made by conventional extrusion, with a dip-coated 20 μm thick gas-tight dense layer. Permeation data were not reported.

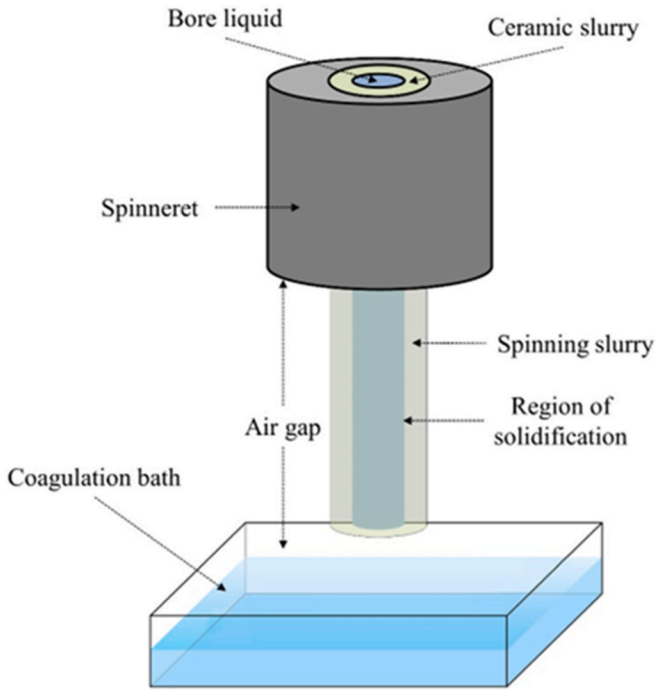

Fig. 12. Schematic representation of a hollow fiber spinneret. Reproduced from Ref. [137].

Several examples of hollow fiber-shaped hydrogen separation membranes have been reported in the literature, over the past decades. Liu et al. [142] successfully produced a dense single-phase $BaCe_{0.8}Y_{0.2}O_{3-\alpha}$ (BCY) hollow fiber membrane (~200 μm-thick, 25 cm-long) exploiting the extrusion-phase inversion technique. The resulting H_2 fluxes were 15 times higher than that of BCY disk-shaped and dry-pressed membranes, with a maximum flux of 0.38 mL cm^{-2} min^{-1} (at 1050 °C with sweep gas flow of 30 mL min^{-1}). The improved performance was attributed to a combination of the 5 times lower thickness of the hollow fiber compared to BCY pellet, with the possibility of reaching higher permeation temperatures (*i.e.,* 1050 °C) for the fiber configuration; such structure entails relatively easier membrane sealing, with the two sealing ends kept away from the high-temperature zone, thus allowing to sustain higher operating temperatures.

The same authors applied the extrusion-phase inversion approach to obtain an asymmetric $BaCe_{0.85}Tb_{0.05}Co_{0.10}O_{3-\delta}$ (BCTCo) perovskite hollow fiber membrane [143]. The outer and inner diameters of the hollow fibers were 1.70 and 1.08 mm, respectively, while the outside dense layer had a thickness of around 132 μm. They also explored the use of Ni and Pd catalytic nanoparticles deposited on both fiber sides, reaching H_2 fluxes of respectively 0.269 mL cm^{-2} min^{-1} and 0.42 mL cm^{-2} min^{-1} at 1000 °C. More recently the authors reported a multi-phase dual-layer $BaCe_{0.8}Y_{0.2}O_{3-\delta}$ (BCY)–$Ce_{0.8}Y_{0.2}O_{2-\delta}$ (YDC)/B-CY-Ni hollow fiber membrane obtained by a single-step co-spinnig and co-sintering method [144], similarly to what reported in Fig. 12. The prepared membrane was composed by a thin densified dual-phase (BCY-YDC) layer supported on a porous catalytic BCY-Ni substrate to minimize the bulk diffusion and enhances the surface exchange rate, and more importantly to provide a good integration between the dense and porous support layers. The thickness of the dense layer could be well controlled by the powder content of BCY- YDC in the spinning suspension, going from 33.5 to 14.5 μm when the content of BCY-YDC was lowered from 65 to 45 wt%. After reducing NiO into Ni, the support layer turned into a highly porous structure which was catalytically active toward the hydrogen decomposition reaction (Fig. 13a–c). An optimized ultrathin dense layer of 17.0 μm and a great adhesion between the separation and porous catalytic support layers were achieved. The as-obtained asymmetric membrane registered an oxygen permeation of 0.566 mL $cm^{-2}min^{-1}$ at 900 °C (50%H_2–He/N_2 as feed/sweep).

3.4.2. Oxygen membranes

Some examples of tubular membranes have been fabricated by plastic extrusion for oxygen separation [145]. In 2007 Zhang et al. [145] documented a mixed-conducting thin tubular membrane made of Al_2O_3-doped $SrCo_{0.8}Fe_{0.2}O_{3-\delta}$ and obtained by a plastic extrusion process. In their work, the authors showed how controlling the weight ratio

Table 5
Hydrogen and oxygen permeation ceramic membranes and relative performances for the extruded systems reported in the literature. Bold systems indicate active (dense) layers whereas italic is used for supports.

Extrusion								
Hydrogen separation membranes								
System	Architecture	Configuration	Extruded part	Thickness [mm]	J [mL cm^{-2} min^{-1}]	Feed/ Sweep gasses	T [°C]	Ref.
$La_{28-y}W4_{+y}O_{54+\delta}$ (y = 0.848) *-LWO*, **$La_{28-y}W_{4+y}O_{54+\delta}$ (y = 1)** *-LWO* **and $La_{28-y}(W_{1-x}Mo_x)_{4+y}O_{54+\delta}$ (x = 0.3, y = 1)** *-LWMoO*	tubular	Single-phase – asymmetric	support (dense layer *via* dip coating)	0.020 (dense layer)	–	–	–	[141]
$BaCe_{0.8}Y_{0.2}O_{3-\alpha}$ (BCY)	hollow fiber	Single-phase -symmetric	dense (entire membrane)	0.4	0.38	25 % H2–He/ N2	1050	[142]
$BaCe_{0.85}Tb_{0.05}Co_{0.10}O_{3-\delta}$ (BCTCo)-*(BCTCo)*	hollow fiber	Single-phase – asymmetric	dense-porous support	0.132 (dense layer)	0.42	50% H_2–He/ N_2	1000	[143]
$BaCe_{0.8}Y_{0.2}O_{3-\delta}$ (BCY)–$Ce_{0.8}Y_{0.2}O_{2-\delta}$ (YDC)- *(BCY-Ni)*	hollow fiber	Dual-phase – asymmetric	dense- porous support	0.017 (dense layer)	0.566	50% H_2–He/ N_2	900	[144]
Oxygen separation membranes								
Al_2O_3-doped $SrCo_{0.8}Fe_{0.2}O_{3-\delta}$ (SCFA) – *SCFA*	tubular	Single-phase -symmetric	dense (entire membrane)	0.45	1.1	Air/He	900	[145]
$Ba_{0.5}Sr_{0.5}Co_{0.8}Fe_{0.2}O_{3-\delta}$ (BSCF)	tubolar	Single phase -symmetric	dense (entire membrane)	1	2.33	Air/He	950	[146]
$Ba_{0.5}Sr_{0.5}Co_{0.8}Fe_{0.2}O_{3-\delta}$ (BSCF) – *BSCF*	hollow fiber	Single-phase-symmetric	dense (entire membrane)	0.44	5.1	Air/He	950	[150]
$Ce_{0.8}Sm_{0.2}O_{2-\delta}$ (SDC)-$La_{0.7}Ca_{0.3}CrO_{3-\delta}$ (LCC) – *(SDC-LCC)*	hollow fiber	Dual-phase - asymmetric	dense-support	0.2 (dense layer)	2.3×10^{-7} mol · cm^{-2}· s^{-1}	Air/He	950	[151]
$Gd_{0.2}Ce_{0.8}O_{2-\delta}$ - $La_{0.6}Sr_{0.4}Co_{0.2}Fe_{0.8}O_{3-\delta}$(GDC-LSCF) – *(GDC-LSCF)*	hollow fiber	Dual-phase - asymmetric	support (dense layer *via* dip coating)	0.015 (dense layer)	2.68	Air/He	900	[152]

of the ceramic powder to the polymer binder (PVA), a thin tubular symmetric membrane is produced (outer diameter ~ 2.6 mm, inner diameter ~1.7 mm, 0.45 mm thickness) achieving an oxygen flux of 1.1 mL $min^{-1}cm^{-2}$ at 900 °C (Air/He as feed/sweep).

Gromada et al. [146] reported thin-walled tubular $Ba_{0.5}Sr_{0.5}Co_{0.8}Fe_{0.2}O_{3-\delta}$ (BSCF) membranes prepared at the pilot-scale level mixing methylcellulose suspension and BSCF powder. After the extrusion process, green tubes with lengths of approximately 600 mm, and external and internal diameters of 23.4 and 17.4 mm respectively were obtained, producing a 1.0 mm-thick membrane after sintering. An oxygen permeation flux of 2.33 mL $min^{-1}cm^{-2}$ was obtained at 950 °C under 2 dm^3 min^{-1} airflow and 5 dm^3 min^{-1} of helium flow, confirming extrusion as an attractive method to manufacture industrial-scale membranes for oxygen separation.

Recently, the mechanical stability of asymmetric BSCF tubular membranes was improved by the adaption of extrusion parameters and sintering conditions by Hoffmann et al. [147,148]. The study revealed a remarkably improved long-term stability for supports manufactured using novel extrusion parameters and reduced firing temperatures. The oxygen permeation increased with rising grain size in the membrane layer, especially at high temperatures. An increased oxygen permeation (~3 mL min^{-1} cm^{-1}) at temperatures below 750 °C, was found for this system.

The possibility to further improve the performances of the membranes by reducing the membrane wall thickness has pushed the research toward the fabrication of hollow fibers. In 2005 Liu and Gavalas [149] fabricated an oxygen ion conducting $Ba_{0.5}Sr_{0.5}Co_{0.8}Fe_{0.2}O_{3-\delta}$ hollow fiber membrane through a sequence of extrusion, gelation, and sintering. The BSCF powder was dispersed in a polymer solution and extruded through a spinnerette. An additional dip coating step was implemented to achieve a thin BSCF coating on the external surface of the fiber [150]. The membrane, which could be in this way tested,

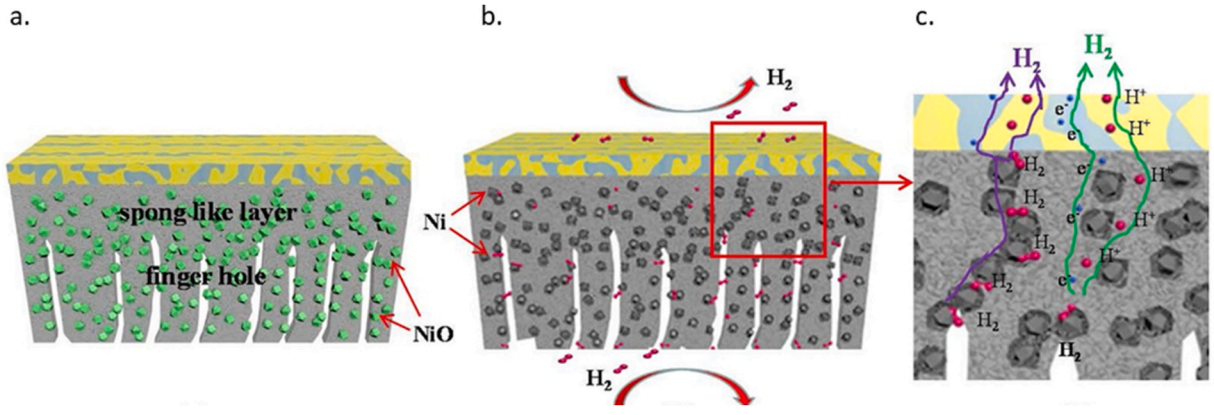

Fig. 13. Schematic illustration of BCY-YDC/BCY-Ni hollow fiber membrane structure and H_2 permeation process through the membrane: (a) Before reduction; (b) After reduction; and (c) H_2 permeation process. Reproduced from Ref. [144].

achieved a maximum oxygen flux of 5.1 mL $min^{-1}cm^{-2}$ at 950 °C (Air/He as feed/sweep).

Tian et al. [151] proposed a $Ce_{0.8}Sm_{0.2}O_{2-\delta}$ (SDC)-$La_{0.7}Ca_{0.3}CrO_{3-\delta}$ (LCC) dual-phase composite hollow fiber with a wall thickness of 0.2 mm prepared by the phase-inversion/extrusion method employing individual metal oxides and carbonates as starting materials. A gas-tight separation membrane was obtained after sintering which registered under an air feed (shell side), an oxygen permeation of $2.3 \cdot 10^{-7}$ mol cm^{-2} s^{-1} at 950 °C (He into the lumen).

Wu et al. [86] conducted a study on the effect of the separation layer thickness on the oxygen permeation and mechanical strength in a series of $La_{0.80}Sr_{0.20}MnO_{3-\delta}$ (LSM)-Scandia(10 %)-Stabilized-Zirconia (ScSZ)/ScSZ-NiO functional dual-layer hollow fibers prepared *via* a single step co-extrusion and co-sintering process. The change in thickness of the external side of the membrane was achieved by varying the extrusion rate of the outer layer while maintaining the rate of the inner one fixed. As the major contribution to the mechanical strength of the dual-layer hollow fibers derived from the inner substrate layer, thicker external layers resulted in weaker membranes; the increasing extrusion rate of the outer layer led to a consequent reduction in thickness of the substrate (inner layer) therefore undermining the membrane mechanical stability.

Ren et al. [152] reported a novel process to fabricate a multilayer asymmetric hollow fiber membrane with a rational design using 67 vol % $Gd_{0.2}Ce_{0.8}O_{2-\delta}$ − 33 vol % $La_{0.6}Sr_{0.4}Co_{0.2}Fe_{0.8}O_{3-\delta}$ (GDC-LSCF) as a model material system. The phase inversion-based extrusion process was employed to fabricate a hollow fiber substrate featuring radially well--aligned microchannels open at the inner surface (Fig. 14b and c). A thin dense separation layer and a porous surface catalyst layer at the shell side were then produced by dip-coating and sintering (Fig. 14a). The as-obtained system registered an oxygen permeation flux of 2.68 mL min^{-1} cm^{-2} at 900 °C under Ar/air gradient. This work demonstrated that the coupling of dip coating with the extrusion can be used to obtain dense functional layers without recurring to high sintering temperatures. Those are usually required to densify the separation layer in a conventional extrusion process with the risk of destroying the desired porous microstructures in the supporting element.

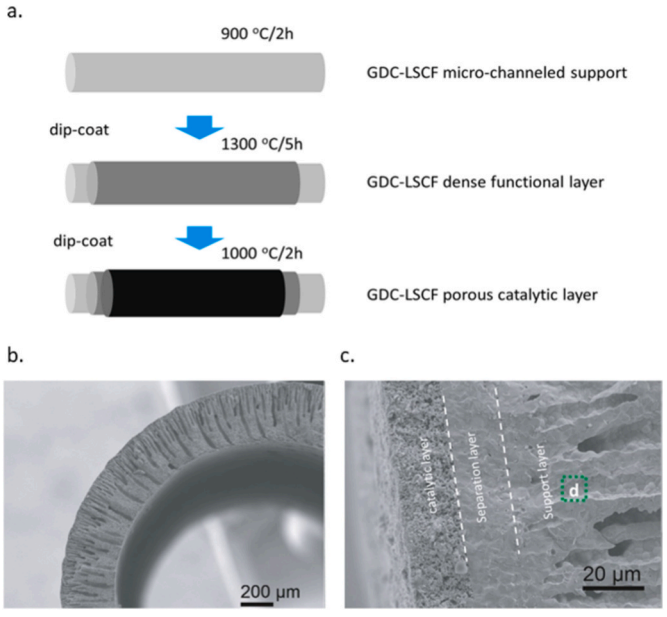

Fig. 14. Illustration of multi-layer GDC-LSCF membrane fabrication process (a); SEM cross-sectional image (b) and enlarged image near the interfaces of the sintered hollow fiber membrane (c). Modified from Ref. [153].

3.5. Dry pressing

Dry compaction is the most popular shape-forming process to obtain thick gas membranes since it involves a relatively simple and cost-effective technology allowing high production rates [154]. Dry pressing implies compacting a nominally dry powder (*i.e.,* < 2 wt% water) in a mold or die at pressures of 21–690 MPa (3000–100000 psi). This pressure should be high enough to produce a homogeneous green compact with sufficient strength for subsequent handling/processing, but low enough to avoid excessive wear on the press and tooling (*i.e.*, the forming die/mold). To improve handling and processability, ceramic powders are typically granulated with 1–5 wt.% organic binder for dry pressing [155].

Although this technique is by far the most exploited on the laboratory scale, it suffers from several technical issues which make it difficult to be scaled-up, and therefore it is not appropriate for mass production of thin large area membranes. One of the major drawbacks is related to the difficulty in controlling the uniform distribution of the powder for layers as thin as 20 μm, making it not appropriate for the preparation of thin membranes [156]. Another disadvantage consists in the inhomogeneous density of green compacts, which results in warpage and crack during sintering [157]. This method has been widely used for the fabrication of dense symmetric disk-shaped membranes (*i.e.* pellets) for both hydrogen and oxygen separation as it is frequently considered a fast and simple way to prepare testable membranes of new materials. Nevertheless, asymmetric architectures are also reported, and by optimizing the physical-chemical property of the powder (*i.e.* granulometry, packing density, etc.) it is possible to obtain asymmetric architecture with dense active layers of only a few tens of micrometers. In the next two paragraphs particular attention will be given to the strategies allowing the achievement of asymmetric structure highlighting the major challenges related to the ceramic process. Hydrogen and oxygen systems produced using this technique were summarized in Table 6.

3.5.1. Hydrogen membranes

E. Rebollo et al. [158] reported the fabrication of a symmetric hydrogen membrane made by dry-pressing a 50:50 vol ratio mixture of $BaCe_{0.65}Zr_{0.2}Y_{0.15}O_{3-\delta}$ and $Ce_{0.85}Gd_{0.15}O_{2-\delta}$ (BCZ20Y15-GDC15). The resulting dense disk-shaped membrane of 0.65 mm thickness reached a hydrogen flux as high as 0.27 mL min^{-1} cm^{-1} at 755 °C when the feed and the sweep sides of the membrane were hydrated (*i.e.,* humidified 50 % H_2 in He/humidified Ar for feed and sweep respectively) which was one of the highest hydrogen fluxes obtained for bulk ceramic membranes and therefore deserves to be mentioned.

Asymmetric proton-conducting $SrCe_{0.95}Tm_{0.05}O_{3-\delta}$ (SCTm) membranes consisting of a dense thin film and a thick, porous support of the same material were prepared *via* the dry pressing method by Chen et al. [159]. To achieve an asymmetric structure two different particle sizes were employed: smaller particle size powder (*i.e.,* 0.2 μm) was used to make the dense top layer while larger particle size powder (*i.e.,* 7 μm) was exploited to produce the porous substrate (Fig. 15).

The particle size of the powder was revealed to be an important factor that affects the porosity and shrinkage of the sintered disks. As the average particle size of the powder increased, the shrinkage of the membrane decreased thus producing an increase in porosity till a critical value was reached above which the disk gets laminated after sintering. A minimum thickness of 150 μm was achieved for the dense layer, registering a hydrogen flux of 9.37×10^{-8} mol $cm^{-2}s^{-1}$ at 900 °C when 10 % H_2/He and air were used at the upstream and downstream side, respectively.

Zhan et al. [160] successfully employed this cost-effective method for the fabrication of asymmetrical thin (50 μm) $SrCe_{0.95}Y_{0.05}O_{3-\delta}$ (SCY) membranes controlling the thickness of the active layer by varying the powder amount. The substrate consisted of SCY, NiO and soluble starch, while the top layer was the SCY. NiO was used to generate porosity when reduced to Ni by the hydrogen flux at high temperatures and for its

Table 6
Hydrogen and oxygen permeation ceramic membranes and relative performances for dry-pressed systems reported in the literature. Bold systems indicate active (dense) layers whereas italic is used for supports.

Dry-pressing								
Hydrogen separation membranes								
System	Architecture	Configuration	Dry-pressed part	Thickness [mm]	J [mL cm^{-2} min^{-1}]	Feed/Sweep gasses	T [°C]	Ref.
$BaCe_{0.65}Zr_{0.2}Y_{0.15}O_{3-\delta}$ (BCZ20Y15) –$Ce_{0.85}Gd_{0.15}O_{2-\delta}$ (GDC15)	disk	Dual-phase - symmetric	dense (entire membrane)	0.65	0.27	wet 50% H_2–He/wet Ar	755	[158]
$SrCe_{0.95}Tm_{0.05}O_{3-\delta}$ (SCTm) – *SCTm*	disk	Single-phase – asymmetric	dense-support	0.150 (dense layer)	9.37 × 10^{-8} mol $cm^{-2}s^{-1}$	10%H_2–He/ Air	900	[159]
$SrCe_{0.95}Y_{0.05}O_{3-\delta}$ (SCY) – *SCY*	disk	Single-phase – asymmetric	dense-support	0.050	7.6 × 10^{-8} mol $cm^{-2}s^{-1}$	80%H_2–He/ Ar	950	[160]
$La_{0.5}Ce_{0.5}O_{2-\delta}$ (LDC) - *LDC*	disk	Single-phase – asymmetric	dense-support	0.030	2.6 × 10^{-8} mol $cm^{-2}s^{-1}$	20% H_2–He–3% H_2O/Ar	900	[161]
$BaCe_{0.85}Tb_{0.05}Zr_{0.1}O_{3-\delta}$ (BCTZ) - *BCTZ*	disk	Single-phase – asymmetric	dense-support	0.020	0.35	50%H_2–He/ Ar	1000	[162]
$La_{5.5}(W_{0.6}Mo_{0.4})_{0.95}Pd_{0.05}O_{11.25-\delta}$	disk	Single-phase – symmetric	dense (entire membrane)	0.25	0.4	50%H_2–He/ Ar	800	[163]
$La_{5.5}(W_{0.6}Mo_{0.4})_{0.95}Pd_{0.05}O_{11.25-\delta}$	disk	Single-phase – symmetric	dense (entire membrane)	0.25	1.3	50%H_2–He/ Ar	1000	[163]
Oxygen separation membranes								
$Ba_{0.5}Sr_{0.5}Co_{0.8}Fe_{0.2}O_{3-\delta}$ (BSCF5582) – $Ba_{0.5}Sr_{0.5}Co_{0.2}Fe_{0.8}O_{3-\delta}$ (BSCF5528)	disk	Dual phase-layer structured-symmetric	dense (entire membrane)	0.030 (active layer)	2.1	Air/N_2	900	[164]
$Ba_{0.5}Sr_{0.5}Co_{0.8}Fe_{0.2}O_{3-\delta}$ (BSCF)	tubolar	Single phase -symmetric	dense (entire membrane)	–	1.28	Air/He	950	[146]

excellent chemisorption and catalytic properties. Soluble starch was also used to control the shrinkage of the substrate to match that of the top layer. In this way, crack-free asymmetrical membranes with thin dense active layers were produced which achieved a hydrogen permeation flux of 7.6 × 10^{-8} mol $cm^{-2}s^{-1}$ at 950 °C when a mixture of 80 % H_2/He was used as the feed (Ar as sweep gas).

A $La_{0.5}Ce_{0.5}O_{2-\delta}$ (LDC) hydrogen separation membrane with an asymmetrical structure was fabricated by a co-pressing method, using NiO, LDC, and corn starch mixture for the substrate and LDC as the top membrane active layer [161]; a 30 μm-thick dense layer was in this way

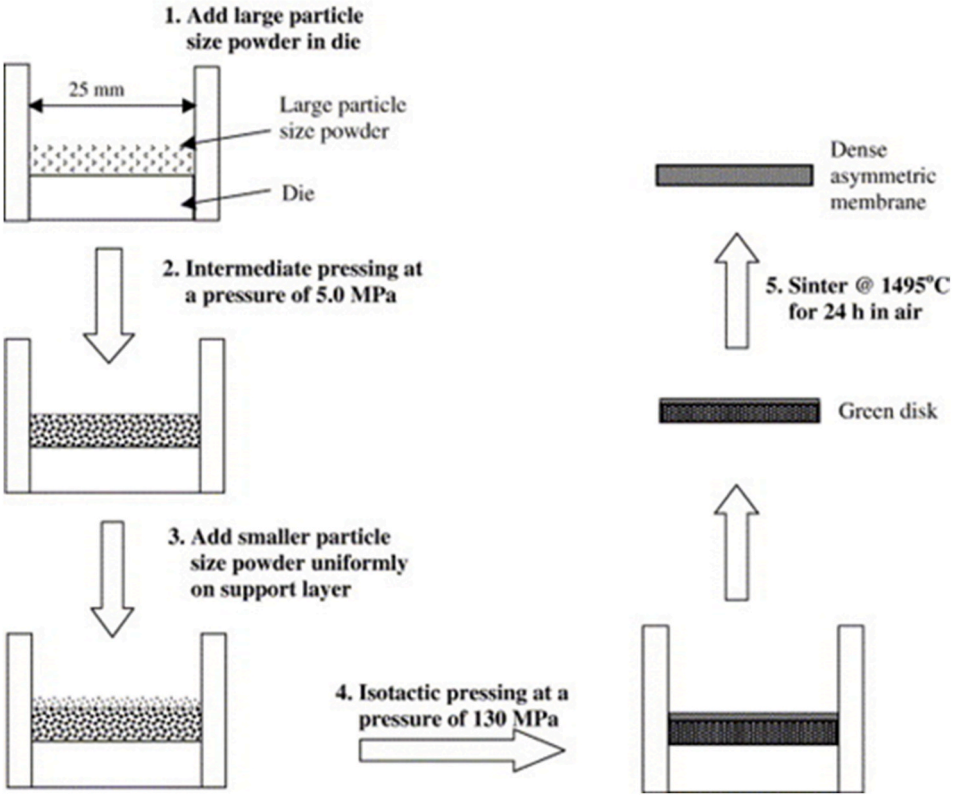

Fig. 15. Illustration of the dry pressing procedure employed for the fabrication of the disk-shaped SCTm asymmetrical membrane. Reproduced from Ref. [159].

Table 7
Hydrogen and oxygen permeation ceramic membranes (and relative performances) produced by combining the dry-pressing method for the porous support with a colloidal process for the dense active layer. Bold systems indicate active (dense) layers whereas italic is used for supports.

Colloidal processes combined with dry pressing								
Hydrogen separation membranes								
System	Architecture	Configuration	Colloidal method for the dense layer	Thickness [mm]	J [mL cm^{-2} min^{-1}]	Feed/Sweep gasses	T [°C]	Ref.
($BaCe_{0.9}Y_{0.1}O_{3-\delta}$ – Zr based alloy)- *ZrO_2*	disk	Dual phase -asymmetric	Aerosol Deposition	0.010	0.17	10%H_2–N_2/ Ar	800	[166]
$SrCe_{0.95}Yb_{0.05}O_{3-\alpha}$ (SCY) – *$SrZr_{0.95}Y_{0.05}O_{3-\alpha}$*	disk	Single phase -asymmetric	Spin Coating	0.002	6×10^{-4} mol cm^{-2} min^{-1}	H_2–N_2/N_2	680	[67]
Oxygen separation membranes								
$Ba_{0.5}Sr_{0.5}Co_{0.8}Fe_{0.2}O_3$.δ (BSCF) – *BSCF*	disk	Single phase -asymmetric	Electrophoretic Deposotion	0.015	2.5	Air/Ar	850	[168]
$Pr_{0.5}Ce_{0.5}O_{2-\delta}$ - $Ba_{0.5}Sr_{0.5}Co_{0.8}Fe_{0.2}O_{3-\delta}$	disk	Dual phase -asymmetric	Wet spray deposition	0.010	1.6	Air/He	850	[167]

achieved in the asymmetric membrane. Using a mixture of 20 % H_2/N_2 (with 3 % of H_2O) as feed gas and dry high-purity argon as sweep gas a permeation hydrogen flux of 2.6×10^{-8} mol cm^{-2} s^{-1} was reached (900 °C).

Wei et al. [162] reported the fabrication of a mixed proton and electron conductor $BaCe_{0.85}Tb_{0.05}Zr_{0.1}O_{3-\delta}$ (BCTZ) membrane obtained using commercial starch as the pore-forming agent. The use of a fine powder (*i.e.,* 0.1–0.2 μm) was found to be beneficial for the obtainment of a thin dense layer *via* dry-pressing so that an active layer as thin as 20 μm was fabricated. A hydrogen flux of about 0.35 mL $min^{-1}cm^{-2}$ (1000 °C, 50%H_2–He feed, Ar sweep) was registered. Weng et al. [163] reported the obtaining of $La_{5.5}(W_{0.6}Mo_{0.4})_{0.95}Pd_{0.05}O_{11.25-\delta}$ (LWMPd) symmetric membrane showing very high hydrogen permeation flux of 1.3 mL min^{-1} cm^{-2} at 1000 °C. The addition of noble metals to the ceramic materials is recognized an effectively strategy to improve the ceramic membrane performances; particularly, addition and/or decoration with nanoparticles can lead highly gas fluxes maintaining the cost of the membrane acceptable for industrial applications.

3.5.2. Oxygen membranes

An asymmetric dense membrane for oxygen separation made of a dense $Ba_{0.5}Sr_{0.5}Co_{0.2}Fe_{0.8}O_{3-\delta}$ thin-film layer on top of a dense thick $Ba_{0.5}Sr_{0.5}Co_{0.8}Fe_{0.2}O_{3-\delta}$ support was fabricated by Chen et al. [164]. A dual-layered membrane with an active layer thickness down to 10 μm was fabricated thanks to the use of a BSFC powder with an ultra-low packing density. The oxygen permeation test performed on a 30 μm-thick membrane registered a value of 2.1 mL $min^{-1}cm^{-2}$ (900 °C, Air/N_2 as feed/sweep).

Gromada et al. [146] reported the use of dry-pressing for the $Ba_{0.5}Sr_{0.5}Co_{0.8}Fe_{0.2}O_{3-\delta}$ tubular membrane fabrication. Manufacturing tubular membranes by this method required determining the optimal parameters for pressing, turning the semi-product on the lathe, developing the sintering treatment, and finally grinding the sintered membrane. To improve the mouldability, granulated raw starting material prepared by means of a spray drier was used. An oxygen flux of 1.28 ml cm^{-2} min^{-1} (950 °C, Air/He) was achieved which was lower than the one obtained by an extruded tubular membrane in the same operating condition.

Jiang et al. [165] conducted a study on the oxygen permeation properties of single-phase asymmetric $Ba_{0.5}Sr_{0.5}Co_{0.8}Fe_{0.2}O_x$ (BSCF) membranes produced by means of a dry-pressing method employing ethyl-cellulose powders and carbon fiber as pore formers for the porous layer. As compared to BSCF dense membranes used as a reference, the oxygen fluxes of BSCF asymmetric membranes were significantly enhanced because of the decrease in the constraining effect of bulk diffusion on the permeation.

3.5.3. Colloidal processes combined with dry pressing

A few examples of colloidal processes coupled with dry pressing can be found in literature to produce asymmetric membranes on the laboratory scale. These methods are based on the preparation of a suitable ceramic suspension to be deposited as thin active layers onto porous supports produced by dry pressing. The as-obtained bilayer structure is finally cofired to obtain the correspondent asymmetric systems. Aerosol [166]/wet spray [167] deposition, electrophoretic deposition [168], and spin-coating [67] techniques have been employed in the preparation of thin dense active layers for separation membranes. The few examples available with the relative performances are listed in Table 7. Clearly, more research is needed to effectively evaluate and push the applicability of these processes to the fabrication of robust gas separation membranes.

4. Conclusion and future Trends

Hydrogen and oxygen are considered crucial gasses for several industrial processes and fundamental energy carriers to reach the climate-neutral economy targeted by the European Green Deal. The development of dense ceramic membrane technology, where gaseous species are transported through a pressure-driven mode, opens the possibility to supply gases that are theoretically 100 % pure. This capability enables the direct implementation of this technology in high-temperature plants (500–900 °C) with a consequent reduction of the production cost, ensuring at the same time a higher chemical and thermal stability.

An asymmetric configuration of these systems enhances gas permeation by reducing bulk diffusion resistance while retaining good mechanical stability. This is achieved through the combination of a dense, thin active layer with a porous, thicker substrate.

The most promising oxygen separation membranes are constituted by perovskites with ambipolar anionic-electronic conductivity eventually mixed with an additional electronic conductor forming a dual-phase system that is able to provide sufficiently high oxygen fluxes at high temperatures (>700 °C). Despite the most effective materials are well-established [169], a real advancement in terms of industrial application for the development of oxygen separation technology is expected only considering a fine-tuning of the membrane microstructure and architecture able to reach superior permeabilities.

Mixed protonic-electronic conductors have been intensively studied for dense ceramic hydrogen separation membranes thanks to their high mechanical, chemical, and thermal stability, and lower manufacturing cost compared to their dense metallic counterparts. However, the degree of advancement of this technology is lower than the oxygen separation one. Despite the numerous recent research findings on new performing protonic-electronic conducting compositions, the state-of-the-art permeability of these membranes is lower than the one achieved by ceramic-based systems for oxygen permeation. Nevertheless, for both

hydrogen and oxygen membranes, the optimization of manufacturing processes for asymmetric architectures remains a key requirement to achieve increased gas permeability and reliable components on a mass-production scale [169].

Different membrane architectures, *i.e.,* planar, tubular and hollow fibers, have been developed, each offering specific advantages and meeting particular requirements based on the final application [58]. Nonetheless, the planar geometry is the most considered for laboratory studies on materials optimization.

For oxygen separation planar membranes, plenty of different manufacturing processes have been explored. The most used technique remains the conventional dry pressing of powder. This manufacturing process is mainly applied for the development of symmetric architectures even if some examples of dense-porous structures have been reported in the literature for MIEC compositions. Nevertheless, the poor thickness control (minimum thickness of about 20 μm) and the limited scalability make dry pressing mainly suitable for laboratory scale asymmetric membranes studies.

To produce planar architectures, tape casting is the most used method allowing the fabrication of multilayer membranes by co-lamination of different tapes or even co-tape casting. The use of this technique has been extensively reported over the years thanks to its large flexibility in terms of size and thickness of the produced substrates which allows the production of large, flat, and thin devices that could not otherwise be manufactured by dry pressing. Tape casting involves the mixing of the two (ionic and electronic) ceramic conductors to produce dense and porous layers that are then stacked and co-sintered, despite some examples of independently distributed phase membranes have been proposed [76–78]. The porous support is generally obtained by introducing a pore-forming agent in the slurry that is removed during the thermal treatment leaving a randomly distributed porosity along the whole support thickness. Despite this is the most straightforward and adopted strategy to produce gas-permeable porosity, it can lead to a moderate gas diffusion resistance of the support. To enable fast gas transportation, phase inversion tape casting was proposed by different authors with the aim of producing directional porosity in the substrates for achieving better permeation fluxes in the final asymmetric system. For the same reason, freeze-cast porous substrates with highly oriented porosity have also been successfully proposed for some perovskites. These engineered supports are then integrated with thin active layers fabricated by other deposition processes such as screen printing, dip-coating, *etc*., obtaining in this way membranes with higher gaseous fluxes.

A hybrid approach, *i.e.* freeze-tape casting, has recently been proposed for oxygen separation systems. This method combines the advantages of both freeze-casting and tape casting, enabling the production of large, flat, and thin layers (characteristic of tape casting) endowed with oriented and aligned porosity (typical of freeze-casting). The generally enhanced oxygen permeation fluxes obtained using these methods clearly indicate the importance of selecting fabrication processes that allow the production of directional porosity. However, further studies need to be conducted in this direction to develop reliable and reproducible manufacturing procedures able to be applied at the industrial level.

Tubular architectures for oxygen separation are a viable alternative, with the peculiar advantage of higher mechanical robustness and an easier sealing compared to planar systems. Tubular geometries are generally produced by the tape casting/rolling method or through extrusion-based techniques. Extrusion is confirmed to be the most attractive method to develop tubular membranes for application on an industrial scale, as compromise between performances, robustness and costs. However, in recent years, the need to further improve the performances of the membranes by reducing the membrane wall thickness has boosted the research towards the fabrication of hollow fibers. This architecture allows the additional advantage of obtaining aligned microchannel porosities when coupled to phase-inversion methods pushing the more conventional tubular architecture towards higher permeation rates.

The same fabrication processes have also been applied to hydrogen separation to produce asymmetric systems. Tubular architecture has been fabricated by tape casting/rolling process or extrusion, and in form of hollow fibers, by modified extrusion technique and co-spinning method. As for oxygen separation membranes, hollow fibers obtained using the phase inversion method allow the obtainment of aligned porosities and good levels of H_2 permeability compared to the results for the same planar systems. Although some examples of asymmetric membranes produced by dry pressing are shown, planar architectures are generally fabricated through tape casting using pore-forming agents to produce porous support, co-laminating the thin dense layer on the top of it. Recently, the development of different compositions and architectures allowed the strong improvement of the H_2 permeation fluxes. Even in the case of H_2, some very recent works have been published on membranes displaying an aligned porosity made by coupling the freeze casting technique for the fabrication of the porous support with screen printing for the thin active layer. In addition, some recent works [170–172] lay the foundations for the exploitation of additive manufacturing methods to improve the design freedom, customization, costs and production time of these systems. Despite these research advancements, studies about new materials, design and optimized process parameters are needed for the ceramic hydrogen separation technology to reach the industrial applicability.

Declaration of competing interest

The authors declare that they have no known competing financial interests or personal relationships that could have appeared to influence the work reported in this paper.

Data availability

No data was used for the research described in the article.

Acknowledgement

This research did not receive any specific grant from funding agencies in the public, commercial, or not-for-profit sectors.

References

[1] Chapman A, Itaoka K, Farabi-Asl H, Fujii Y, Nakahara M. Societal penetration of hydrogen into the future energy system: Impacts of policy, technology and carbon targets. Int J Hydrogen Energy 2020;45:3883–98. https://doi.org/10.1016/j.ijhydene.2019.12.112.

[2] Hanley ES, Deane J, Bó Gallachóir. The role of hydrogen in low carbon energy futures–A review of existing perspectives. Renew Sustain Energy Rev 2018;82:3027–45. https://doi.org/10.1016/j.rser.2017.10.034.

[3] Lebrouhi BE, Djoupo JJ, Lamrani B, Benabdelaziz K, Kousksou T. Global hydrogen development - a technological and geopolitical overview. Int J Hydrogen Energy 2022;47:7016–48. https://doi.org/10.1016/j.ijhydene.2021.12.076.

[4] Zou C, Zhao Q, Zhang G, Xiong B. Energy revolution: from a fossil energy era to a new energy era. Nat Gas Ind B 2016;3:1–11. https://doi.org/10.1016/j.ngib.2016.02.001.

[5] Mustafa A, Lougou BG, Shuai Y, Wang Z, Tan H. Current technology development for CO2 utilization into solar fuels and chemicals: a review. J Energy Chem 2020;49:96–123. https://doi.org/10.1016/j.jechem.2020.01.023.

[6] Yalcin S, Konukman A, Midilli A. Present and future of flue gas emission reduction technologies related to fossil power generation. GREENHOUSE GASES-SCIENCE AND TECHNOLOGY 2020;10. https://doi.org/10.1002/ghg.1952.

[7] Edwards PP, Kuznetsov VL, David WIF, Brandon NP. Hydrogen and fuel cells: towards a sustainable energy future. Energy Pol 2008;36:4356–62. https://doi.org/10.1016/j.enpol.2008.09.036.

[8] Staffell I, Scamman D, Abad AV, Balcombe P, Dodds PE, Ekins P, et al. The role of hydrogen and fuel cells in the global energy system. Energy & Environmental Science Sci 2019;12:463–91. https://doi.org/10.1039/C8EE01157E.

[9] De Vrieze J, Verbeeck K, Pikaar I, Boere J, Van Wijk A, Rabaey K, et al. The hydrogen gas bio-based economy and the production of renewable building block chemicals, food and energy. New Biotechnology 2020;55:12–8. https://doi.org/10.1016/j.nbt.2019.09.004.

[10] Introduction and Fundamentals. Fundamentals of industrial catalytic processes. John Wiley & Sons, Ltd; 2005. p. 3–59. https://doi.org/10.1002/9780471730071.ch1.

[11] Kent JA, Bommaraju TV, Barnicki SD, editors. Handbook of industrial Chemistry and Biotechnology. Cham: Springer International Publishing; 2017. https://doi.org/10.1007/978-3-319-52287-6.

[12] Ramachandran R, Menon RK. An overview of industrial uses of hydrogen. Int J Hydrogen Energy 1998;23:593–8. https://doi.org/10.1016/S0360-3199(97)00112-2.

[13] Lloyd L. Handbook of industrial catalysts. Boston, MA: Springer US; 2011. https://doi.org/10.1007/978-0-387-49962-8.

[14] El-Shafie M, Kambara S, Hayakawa Y. Hydrogen production technologies overview. 2019.

[15] Kalamaras CM, Efstathiou AM. Hydrogen production technologies: Current state and future developments. Conference Papers in Science 2013;2013:e690627. https://doi.org/10.1155/2013/690627.

[16] Rostrup-nielsen J, Christiansen LJ. Concepts in syngas manufacture. World Scientific 2011;10:3–4.

[17] Bouwmeester HJM, Burggraaf AJ. Chapter 10 Dense ceramic membranes for oxygen separation. In: Burggraaf AJ, Cot L, editors. Membrane science and technology, vol. 4. Elsevier; 1996. p. 435–528. https://doi.org/10.1016/S0927-5193(96)80013-1.

[18] Heidenreich S, Müller M, Foscolo P. In: Advanced process combination concepts; 2016. p. 55–97. https://doi.org/10.1016/B978-0-12-804296-0.00005-1.

[19] Guo K, Shi W, Wu D. Experiment research and Simulation analysis of Regenerative oxygen-enriched combustion technology. Energy Proc 2015;66:221–4. https://doi.org/10.1016/j.egypro.2015.02.031.

[20] Hone CA, Kappe CO. The Use of molecular oxygen for liquid phase Aerobic oxidations in continuous flow. In: Noël T, Luque R, editors. Accounts on sustainable flow Chemistry. Cham: Springer International Publishing; 2020. p. 67–110. https://doi.org/10.1007/978-3-030-36572-1_3.

[21] Agrawal R, White TR, Herron DM. Production of ultra-high purity oxygen from cryogenic air separation plants. 1998. EP0762066A3.

[22] Wang B, Zhou R, Yu L, Qiu L, Zhi X, Zhang X. Evaluation of mass transfer correlations applying to cryogenic distillation process with non-equilibrium model. Cryogenics 2019;97:22–30. https://doi.org/10.1016/j.cryogenics.2018.11.010.

[23] Yousef AM, El-Maghlany WM, Eldrainy YA, Attia A. New approach for biogas purification using cryogenic separation and distillation process for CO2 capture. Energy 2018;156:328–51. https://doi.org/10.1016/j.energy.2018.05.106.

[24] Klimkowicz A, Cichy K, Chmaissem O, Dabrowski B, Poudel B, Świerczek K, et al. Reversible oxygen intercalation in hexagonal Y0.7Tb0.3MnO3+δ: toward oxygen production by temperature-swing absorption in air. J Mater Chem A 2019;7:2608–18. https://doi.org/10.1039/C8TA09235D.

[25] Kim M-B, Jee J-G, Bae Y-S, Lee C-H. Parametric study of pressure swing adsorption process to purify oxygen using carbon molecular sieve. Ind Eng Chem Res 2005;44:7208–17. https://doi.org/10.1021/ie049032b.

[26] Relvas F, Whitley RD, Silva C, Mendes A. Single-stage pressure swing adsorption for producing fuel cell Grade hydrogen. Ind Eng Chem Res 2018;57:5106–18. https://doi.org/10.1021/acs.iecr.7b05410.

[27] Ye F, Ma S, Tong L, Xiao J, Bénard P, Chahine R. Artificial neural network based optimization for hydrogen purification performance of pressure swing adsorption. Int J Hydrogen Energy 2019;44:5334–44. https://doi.org/10.1016/j.ijhydene.2018.08.104.

[28] Shukla A, Sahoo S, Moharir AS. Non-isothermal Multi-cell Model for pressure swing adsorption process. Int J Hydrogen Energy 2017;42:5150–67. https://doi.org/10.1016/j.ijhydene.2016.11.200.

[29] Belaissaoui B, Le Moullec Y, Hagi H, Favre E. Energy efficiency of oxygen enriched air production technologies: Cryogeny vs membranes. Separ Purif Technol 2014;125:142–50. https://doi.org/10.1016/j.seppur.2014.01.043.

[30] Al-Mufachi NA, Rees NV, Steinberger-Wilkens R. Hydrogen selective membranes: a review of palladium-based dense metal membranes. Renew Sustain Energy Rev 2015;47:540–51. https://doi.org/10.1016/j.rser.2015.03.026.

[31] Zhu X, Shi Y, Li S, Cai N. Two-train elevated-temperature pressure swing adsorption for high-purity hydrogen production. Appl Energy 2018;229:1061–71. https://doi.org/10.1016/j.apenergy.2018.08.093.

[32] Bernardo G, Araújo T, da Silva Lopes T, Sousa J, Mendes A. Recent advances in membrane technologies for hydrogen purification. Int J Hydrogen Energy 2020;45:7313–38. https://doi.org/10.1016/j.ijhydene.2019.06.162.

[33] Jee J-G, Kim M-B, Lee C-H. Pressure swing adsorption processes to purify oxygen using a carbon molecular sieve. Chem Eng Sci 2005;60:869–82. https://doi.org/10.1016/j.ces.2004.09.050.

[34] Hashim SS, Mohamed AR, Bhatia S. Oxygen separation from air using ceramic-based membrane technology for sustainable fuel production and power generation. Renew Sustain Energy Rev 2011;15:1284–93. https://doi.org/10.1016/j.rser.2010.10.002.

[35] Yin H, Yip ACK. A review on the production and purification of Biomass-derived hydrogen using emerging membrane technologies. Catalysts 2017;7:297. https://doi.org/10.3390/catal7100297.

[36] Wang H, Wang X, Meng B, Tan X, Loh KS, Sunarso J, et al. Perovskite-based mixed protonic–electronic conducting membranes for hydrogen separation: recent status and advances. J Ind Eng Chem 2018;60:297–306. https://doi.org/10.1016/j.jiec.2017.11.016.

[37] Nunes SP, Culfaz-Emecen PZ, Ramon GZ, Visser T, Koops GH, Jin W, et al. Thinking the future of membranes: perspectives for advanced and new membrane materials and manufacturing processes. J Membr Sci 2020;598:117761. https://doi.org/10.1016/j.memsci.2019.117761.

[38] Saidi M. Application of catalytic membrane reactor for pure hydrogen production by flare gas recovery as a novel approach. Int J Hydrogen Energy 2018;43:14834–47. https://doi.org/10.1016/j.ijhydene.2018.05.156.

[39] Bouwmeester HJM. Dense ceramic membranes for methane conversion. Catal Today 2003;82:141–50. https://doi.org/10.1016/S0920-5861(03)00222-0.

[40] Liang F, He G, Jia L, Jiang H. Cobalt-free dual-phase oxygen transporting membrane reactor for the oxidative dehydrogenation of ethane. Separ Purif Technol 2019;211:966–71. https://doi.org/10.1016/j.seppur.2018.10.055.

[41] Wang Z, Bian Z, Dewangan N, Xu J, Kawi S. High-performance catalytic perovskite hollow fiber membrane reactor for oxidative propane dehydrogenation. J Membr Sci 2019;578:36–42. https://doi.org/10.1016/j.memsci.2019.02.012.

[42] Wang B, Bi L, Zhao XS. Fabrication of one-step co-fired proton-conducting solid oxide fuel cells with the assistance of microwave sintering. J Eur Ceram Soc 2018;38:5620–4. https://doi.org/10.1016/j.jeurceramsoc.2018.08.020.

[43] Tarutina LR, Vdovin GK, Lyagaeva JG, Medvedev DA. BaCe0.7–xZr0.2Y0.1FexO3–δ derived from proton-conducting electrolytes: a way of designing chemically compatible cathodes for solid oxide fuel cells. J Alloys Compd 2020;831:154895. https://doi.org/10.1016/j.jallcom.2020.154895.

[44] Richter J, Holtappels P, Graule T, Nakamura T, Gauckler LJ. Materials design for perovskite SOFC cathodes. Monatshefte fur Chemie 2009;140:985–99. https://doi.org/10.1007/s00706-009-0153-3.

[45] Plekhanov MS, Kuzmin AV, Tropin ES, Korolev DA, Ananyev MV. New mixed ionic and electronic conductors based on LaScO3: protonic ceramic fuel cells electrodes. J Power Sources 2020;449:227476. https://doi.org/10.1016/j.jpowsour.2019.227476.

[46] Jeong S, Yamaguchi T, Okamoto M, Zhu C, Habazaki H, Nagayama M, et al. Proton Pumping boosts energy conversion in hydrogen-permeable metal-supported protonic fuel cells. ACS Appl Energy Mater 2020;3:1222–34. https://doi.org/10.1021/acsaem.9b02287.

[47] Wu Y, Li K, Yang Y, Song W, Ma Z, Chen H, et al. Investigation of Fe-substituted in BaZr0.8Y0.2O3-δ proton conducting oxides as cathode materials for protonic ceramics fuel cells. J Alloys Compd 2020;814:152220. https://doi.org/10.1016/j.jallcom.2019.152220.

[48] Zohourian R, Merkle R, Raimondi G, Maier J. Mixed-conducting perovskites as cathode materials for protonic ceramic fuel cells: Understanding the Trends in proton Uptake. Adv Funct Mater 2018;28:1801241. https://doi.org/10.1002/adfm.201801241.

[49] Alqaheem Y, Alomair A, Vinoba M, Pérez A. Polymeric gas-separation membranes for Petroleum Refining. International Journal of Polymer Science 2017;2017:e4250927. https://doi.org/10.1155/2017/4250927.

[50] Beckman IN, Teplyakov VV. Selective gas transfer through binary polymeric systems based on block-copolymers. Adv Colloid Interface Sci 2015;222:70–8. https://doi.org/10.1016/j.cis.2014.10.004.

[51] Zhang J, Cui Y, Qian G. Rational designed metal-organic frameworks for storage and separation of hydrogen and methane. Curr Org Chem n.d.;22:1792–1808.

[52] Cardoso SP, Azenha IS, Lin Z, Portugal I, Rodrigues AE, Silva CM. Inorganic membranes for hydrogen separation. Separ Purif Rev 2018;47:229–66. https://doi.org/10.1080/15422119.2017.1383917.

[53] Khatib SJ, Oyama ST. Silica membranes for hydrogen separation prepared by chemical vapor deposition (CVD). Separ Purif Technol 2013;111:20–42. https://doi.org/10.1016/j.seppur.2013.03.032.

[54] Ockwig NW, Nenoff TM. Membranes for hydrogen separation. Chem Rev 2007;107:4078–110. https://doi.org/10.1021/cr0501792.

[55] Prajapati PK, Kansara AM, Aswal VK, Singh PS. High oxygen permeable Zeolite-4A poly(dimethylsiloxane) membrane for air separation. J Appl Polym Sci 2019;136:48047. https://doi.org/10.1002/app.48047.

[56] Sazali N. A comprehensive review of carbon molecular sieve membranes for hydrogen production and purification. Int J Adv Manuf Technol 2020;107:2465–83. https://doi.org/10.1007/s00170-020-05196-y.

[57] Bredesen R. Palladium-based membranes for hydrogen separation. 1993.

[58] Meulenberg WA, Schulze-Küppers F, Deibert W, Gestel TV, Baumann S. Ceramic membranes: materials – components – potential applications. ChemBioEng Rev 2019;6:198–208. https://doi.org/10.1002/cben.201900022.

[59] Meng Y, Gao J, Zhao Z, Amoroso J, Tong J, Brinkman KS. Review: recent progress in low-temperature proton-conducting ceramics. J Mater Sci 2019;54:9291–312. https://doi.org/10.1007/s10853-019-03559-9.

[60] Hashim SS, Somalu MR, Loh KS, Liu S, Zhou W, Sunarso J. Perovskite-based proton conducting membranes for hydrogen separation: a review. Int J Hydrogen Energy 2018;43:15281–305. https://doi.org/10.1016/j.ijhydene.2018.06.045.

[61] Wu H-C, Nile G, Lin JYS. Mixed-conducting ceramic-carbonate dual-phase membranes: gas permeation and counter-permeation. J Membr Sci 2020;605:118093. https://doi.org/10.1016/j.memsci.2020.118093.

[62] Liguori S, Kian K, Buggy N, Anzelmo BH, Wilcox J. Opportunities and challenges of low-carbon hydrogen via metallic membranes. Prog Energy Combust Sci 2020;80:100851. https://doi.org/10.1016/j.pecs.2020.100851.

[63] Phair JW, Badwal SPS. Materials for separation membranes in hydrogen and oxygen production and future power generation. Sci Technol Adv Mater 2006;7:792–805. https://doi.org/10.1016/j.stam.2006.11.005.

[64] Gallucci F, Fernandez E, Corengia P, van Sint Annaland M. Recent advances on membranes and membrane reactors for hydrogen production. Chem Eng Sci 2013;92:40–66. https://doi.org/10.1016/j.ces.2013.01.008.

[65] Thursfield A, Metcalfe IS. High temperature gas separation through dual ion-conducting membranes. Current Opinion in Chemical Engineering 2013;2:217–22. https://doi.org/10.1016/j.coche.2013.02.001.

[66] Sunarso J, Baumann S, Serra JM, Meulenberg WA, Liu S, Lin YS, et al. Mixed ionic–electronic conducting (MIEC) ceramic-based membranes for oxygen separation. J Membr Sci 2008;320:13–41. https://doi.org/10.1016/j.memsci.2008.03.074.

[67] Hamakawa S, Li L, Li A, Iglesia E. Synthesis and hydrogen permeation properties of membranes based on dense SrCe0.95Yb0.05O3−α thin films. Solid State Ionics 2002;148:71–81. https://doi.org/10.1016/S0167-2738(02)00047-4.

[68] Fontaine M, Norby T, Larring Y, Grande T, Bredesen R. Oxygen and hydrogen separation membranes based on dense ceramic conductors. Membr Sci Technol 2008;13:401–58. https://doi.org/10.1016/S0927-5193(07)13010-2. Elsevier.

[69] Deibert W, Ivanova ME, Meulenberg WA, Vaßen R, Guillon O. Preparation and sintering behaviour of La5.4WO12−δ asymmetric membranes with optimised microstructure for hydrogen separation. J Membr Sci 2015;492:439–51. https://doi.org/10.1016/j.memsci.2015.05.065.

[70] Llosa Tanco MA, Pacheco Tanaka DA. Recent advances on carbon molecular sieve membranes (CMSMs) and reactors. Processes 2016;4:29. https://doi.org/10.3390/pr4030029.

[71] Alique D, Martinez-Diaz D, Sanz R, Calles JA. Review of supported Pd-based membranes preparation by Electroless Plating for ultra-pure hydrogen production. Membranes 2018;8:5. https://doi.org/10.3390/membranes8010005.

[72] Dolan MD, Dave NC, Ilyushechkin AY, Morpeth LD, McLennan KG. Composition and operation of hydrogen-selective amorphous alloy membranes. J Membr Sci 2006;285:30–55. https://doi.org/10.1016/j.memsci.2006.09.014.

[73] Arratibel Plazaola A, Pacheco Tanaka DA, Van Sint Annaland M, Gallucci F. Recent advances in Pd-based membranes for membrane reactors. Molecules 2017;22:51. https://doi.org/10.3390/molecules22010051.

[74] Wei Y, Yang W, Caro J, Wang H. Dense ceramic oxygen permeable membranes and catalytic membrane reactors. Chem Eng J 2013;220:185–203. https://doi.org/10.1016/j.cej.2013.01.048.

[75] Fontaine ML, Larring Y, Bredesen R, Norby T, Grande T. Dense ceramic membranes based on ion conducting oxides. Ann Chimie Sci Matériaux 2007;32:197–212.

[76] Meng B, Wang H, Cheng H, Wang X, Meng X, Sunarso J, et al. Hydrogen permeation performance of dual-phase protonic-electronic conducting ceramic membrane with regular and independent transport channels. Separ Purif Technol 2019;213:515–23. https://doi.org/10.1016/j.seppur.2018.12.068.

[77] Joo JH, Yun KS, Yoo C-Y, Yu JH. Novel oxygen transport membranes with tunable segmented structures. J Mater Chem A 2014;2:8174–8. https://doi.org/10.1039/C4TA01271B.

[78] Yun KS, Yoo C-Y, Yoon S-G, Yu JH, Joo JH. Chemically and thermo-mechanically stable LSM–YSZ segmented oxygen permeable ceramic membrane. J Membr Sci 2015;486:222–8. https://doi.org/10.1016/j.memsci.2015.03.049.

[79] Rosensteel W, Ricote S, Sullivan N. Hydrogen permeation through dense BaCe0.8Y0.2O3−δ – Ce0.8Y0.2O2−δ composite-ceramic hydrogen separation membranes. Int J Hydrogen Energy 2016;41. https://doi.org/10.1016/j.ijhydene.2015.11.053.

[80] Kreuer K-D. Proton conductivity: materials and applications. Chem Mater 1996;8:610–41. https://doi.org/10.1021/cm950192a.

[81] Li C, Chew JJ, Mahmoud A, Liu S, Sunarso J. Modelling of oxygen transport through mixed ionic-electronic conducting (MIEC) ceramic-based membranes: an overview. J Membr Sci 2018;567:228–60. https://doi.org/10.1016/j.memsci.2018.09.016.

[82] Cheng H. Dual-phase mixed protonic-electronic conducting hydrogen separation membranes: a review. Membranes 2022;12:647. https://doi.org/10.3390/membranes12070647.

[83] Wang A, Liang M, Xiang Q, Xue J, Wang H. Mixed oxygen ionic and electronic conducting membrane reactors for pure chemicals production. Chem Ing Tech 2022;94:31–41. https://doi.org/10.1002/cite.202100160.

[84] Chen G, Feldhoff A, Weidenkaff A, Li C, Liu S, Zhu X, et al. Roadmap for sustainable mixed ionic-electronic conducting membranes. Adv Funct Mater 2022;32:2105702. https://doi.org/10.1002/adfm.202105702.

[85] Li K, Tan X, Liu Y. Single-step fabrication of ceramic hollow fibers for oxygen permeation. J Membr Sci 2006;272:1–5. https://doi.org/10.1016/j.memsci.2005.11.053.

[86] Wu Z, Thursfield A, Metcalfe I, Li K. Effects of separation layer thickness on oxygen permeation and mechanical strength of DL-HFMR-ScSZ. J Membr Sci 2012;415–416:229–36. https://doi.org/10.1016/j.memsci.2012.05.003.

[87] Mercadelli E, Gondolini A, Montaleone D, Pinasco P, Sanson A. Innovative strategy for designing proton conducting ceramic tapes and multilayers for energy applications. J Eur Ceram Soc 2021;41:488–96. https://doi.org/10.1016/j.jeurceramsoc.2020.09.016.

[88] Mercadelli E, Sanson A, Pinasco P, Roncari E, Galassi C. Influence of carbon black on slurry compositions for tape cast porous piezoelectric ceramics. Ceram Int 2011;37:2143–9. https://doi.org/10.1016/j.ceramint.2011.03.058.

[89] Mercadelli E, Gondolini A, Pinasco P, Sanson A. Stainless steel porous substrates produced by tape casting. Met Mater Int 2017;23:184–92. https://doi.org/10.1007/s12540-017-6336-2.

[90] Nishihora RK, Rachadel PL, Quadri MGN, Hotza D. Manufacturing porous ceramic materials by tape casting—a review. J Eur Ceram Soc 2018;38:988–1001. https://doi.org/10.1016/j.jeurceramsoc.2017.11.047.

[91] Fundamentals of Inorganic Membrane Science and Technology, Volume 4 - 1st Edition n.d. https://shop.elsevier.com/books/fundamentals-of-inorganic-membrane-science-and-technology/burggraaf/978-0-444-81877-5 (accessed January 23, 2024).

[92] Loeb S, Sourirajan S. Sea water Demineralization by means of an Osmotic membrane. Saline Water Conversion—II 1963;38:117–32. https://doi.org/10.1021/ba-1963-0038.ch009. AMERICAN CHEMICAL SOCIETY.

[93] Fang H, Ren C, Liu Y, Lu D, Winnubst L, Chen C. Phase-inversion tape casting and synchrotron-radiation computed tomography analysis of porous alumina. J Eur Ceram Soc 2013;33:2049–51. https://doi.org/10.1016/j.jeurceramsoc.2013.02.032.

[94] He W, Huang H, Gao J, Winnubst L, Chen C. Phase-inversion tape casting and oxygen permeation properties of supported ceramic membranes. J Membr Sci 2014;452:294–9. https://doi.org/10.1016/j.memsci.2013.09.063.

[95] Yoon H, Song S-J, Oh T, Li J, Duncan KL, Wachsman ED. Fabrication of thin-film SrCe0.9Eu0.1O3−δ hydrogen separation membranes on Ni–SrCeO3 porous tubular supports. J Am Ceram Soc 2009;92:1849–52. https://doi.org/10.1111/j.1551-2916.2009.03103.x.

[96] Li J, Yoon H, Wachsman ED. Hydrogen permeation through thin supported SrCe0.7Zr0.2Eu0.1O3−δ membranes; dependence of flux on defect equilibria and operating conditions. J Membr Sci 2011;381:126–31. https://doi.org/10.1016/j.memsci.2011.07.032.

[97] Oh T, Yoon H, Li J, Wachsman ED. Hydrogen permeation through thin supported SrZr0.2Ce0.8−xEuxO3−δ membranes. J Membr Sci 2009;345:1–4. https://doi.org/10.1016/j.memsci.2009.08.031.

[98] Hung I-M, Chiang Y-J, Jang JS-C, Lin J-C, Lee S-W, Chang J-K, et al. The proton conduction and hydrogen permeation characteristic of Sr(Ce0.6Zr0.4)0.85Y0.15O3−δ ceramic separation membrane. J Eur Ceram Soc 2015;35:163–70. https://doi.org/10.1016/j.jeurceramsoc.2014.08.019.

[99] Montaleone D, Mercadelli E, Escolástico S, Gondolini A, Serra JM, Sanson A. All-ceramic asymmetric membranes with superior hydrogen permeation. Journal Materials Chemistry A 2018;6:15718–27. https://doi.org/10.1039/C8TA04764B.

[100] Mercadelli E, Gondolini A, Montaleone D, Pinasco P, Escolástico S, Serra JM, et al. Production strategies of asymmetric BaCe0.65Zr0.20Y0.15O3-δ – Ce0.8Gd0.2O2-δ membrane for hydrogen separation. Int J Hydrogen Energy 2020;45:7468–78. https://doi.org/10.1016/j.ijhydene.2019.03.148.

[101] Montaleone D, Mercadelli E, Gondolini A, Pinasco P, Sanson A. On the compatibility of dual phase BaCe0.65Zr0.2Y0.15O3-based membrane for hydrogen separation application. Ceram Int 2017;43:10151–7. https://doi.org/10.1016/j.ceramint.2017.05.039.

[102] Mercadelli E, Montaleone D, Gondolini A, Pinasco P, Sanson A. Tape-cast asymmetric membranes for hydrogen separation. Ceram Int 2017;43:8010–7. https://doi.org/10.1016/j.ceramint.2017.03.099.

[103] Montaleone D, Mercadelli E, Gondolini A, Ardit M, Pinasco P, Sanson A. Role of the sintering atmosphere in the densification and phase composition of asymmetric BCZY-GDC composite membrane. J Eur Ceram Soc 2019;39:21–9. https://doi.org/10.1016/j.jeurceramsoc.2018.01.043.

[104] Mercadelli E, Gondolini A, Ardit M, Cruciani G, Melandri C, Escolástico S, et al. Chemical and mechanical stability of BCZY-GDC membranes for hydrogen separation. Separ Purif Technol 2022;289:120795. https://doi.org/10.1016/j.seppur.2022.120795.

[105] Weirich M, Gurauskis J, Gil V, Wiik K, Einarsrud M-A. Preparation of lanthanum tungstate membranes by tape casting technique. Int J Hydrogen Energy 2012;37:8056–61. https://doi.org/10.1016/j.ijhydene.2011.09.083.

[106] Ivanova ME, Deibert W, Marcano D, Escolástico S, Mauer G, Meulenberg WA, et al. Lanthanum tungstate membranes for H2 extraction and CO2 utilization: fabrication strategies based on sequential tape casting and plasma-spray physical vapor deposition. Separ Purif Technol 2019;219:100–12. https://doi.org/10.1016/j.seppur.2019.03.015.

[107] Fontaine M-L, Smith JB, Larring Y, Bredesen R. On the preparation of asymmetric CaTi0.9Fe0.1O3−δ membranes by tape-casting and co-sintering process. J Membr Sci 2009;326:310–5. https://doi.org/10.1016/j.memsci.2008.10.009.

[108] Baumann S, Serra JM, Lobera MP, Escolástico S, Schulze-Küppers F, Meulenberg WA. Ultrahigh oxygen permeation flux through supported Ba0.5Sr0.5Co0.8Fe0.2O3−δ membranes. J Membr Sci 2011;377:198–205. https://doi.org/10.1016/j.memsci.2011.04.050.

[109] Serra JM, Garcia-Fayos J, Baumann S, Schulze-Küppers F, Meulenberg WA. Oxygen permeation through tape-cast asymmetric all-La0.6Sr0.4Co0.2Fe0.8O3−δ membranes. J Membr Sci 2013;447:297–305. https://doi.org/10.1016/j.memsci.2013.07.030.

[110] Schulze-Küppers F, Baumann S, Tietz F, Bouwmeester HJM, Meulenberg WA. Towards the fabrication of La0.98−xSrxCo0.2Fe0.8O3−δ perovskite-type oxygen transport membranes. J Eur Ceram Soc 2014;34:3741–8. https://doi.org/10.1016/j.jeurceramsoc.2014.06.012.

[111] Fedeli P, Drago F, Schulze-Küppers F, Baumann S. Asymmetric LSCF membranes Utilizing commercial powders. Materials 2020;13:614. https://doi.org/10.3390/ma13030614.

[112] Salehi M, Søgaard M, Esposito V, Foghmoes SPV, Persoon ES, Schroeder M, et al. Oxygen permeation and stability study of (La0.6Ca0.4)0.98(Co0.8Fe0.2)O3-δ membranes. J Membr Sci 2017;542:245–53. https://doi.org/10.1016/j.memsci.2017.07.050.

[113] Cao Z, Zhu X, Li W, Xu B, Yang L, Yang W. Asymmetric dual-phase membranes prepared via tape-casting and co-lamination for oxygen permeation. Mater Lett 2015;147:88–91. https://doi.org/10.1016/j.matlet.2015.02.033.

[114] Pirou S, Gurauskis J, Gil V, Søgaard M, Hendriksen PV, Kaiser A, et al. Oxygen permeation flux through 10Sc1YSZ-MnCo2O4 asymmetric membranes prepared by two-step sintering. Fuel Process Technol 2016;152:192–9. https://doi.org/10.1016/j.fuproc.2016.06.019.

[115] Meng Y, He W, Li X, Gao J, Zhan Z, Yi J, et al. Asymmetric La0.6Sr0.4Co0.2Fe0.8O3-δ membrane with reduced concentration polarization prepared by phase-inversion tape casting and warm pressing. J Membr Sci 2017; 533:11–8. https://doi.org/10.1016/j.memsci.2017.03.025.
[116] Huang H, Cheng S, Gao J, Chen C, Yi J. Phase-inversion tape-casting preparation and significant performance enhancement of Ce0.9Gd0.1O1.95–La0.6Sr0.4Co0.2Fe0.8O3−δ dual-phase asymmetric membrane for oxygen separation. Mater Lett 2014;137:245–8. https://doi.org/10.1016/j.matlet.2014.09.016.
[117] Zhang Y, Yuan R, He Z, Gao J, Chen C. Phase inversion tape casting and oxygen permeation properties of supported planar Zr0.84Y0.16O1.92–La0.8Sr0.2Cr0.5Fe0.5O3−δ composite membrane. Solid State Ionics 2016;288:342–6. https://doi.org/10.1016/j.ssi.2015.12.024.
[118] Zhang Y, Yuan R, Gao J, Chen C. Oxygen permeation properties of supported planar Zr0.84Y0.16O1.92-La0.8Sr0.2Cr0.5Fe0.5O3−δ composite membranes. Separ Purif Technol 2016;166:142–7. https://doi.org/10.1016/j.seppur.2016.04.029.
[119] Cheng S, Huang H, Ovtar S, Simonsen SB, Chen M, Zhang W, et al. High-performance microchanneled asymmetric Gd0.1Ce0.9O1.95−δ–La0.6Sr0.4FeO3−δ-based membranes for oxygen separation. ACS Appl Mater Interfaces 2016;8:4548–60. https://doi.org/10.1021/acsami.5b10714.
[120] Yuan R, He W, Zhang Y, Gao J-F, Chen C. Preparation and characterization of supported planar Zr0.84Y0.16O1.92–La0.8Sr0.2Cr0.5Fe0.5O3− composite membrane. J Membr Sci 2015;499. https://doi.org/10.1016/j.memsci.2015.10.066.
[121] Li C, Ban X, Chen C, Zhan Z. Sandwich-like symmetric dual-phase composite membrane with an ultra-thin oxygen separation layer and excellent durability. Solid State Ionics 2020;345:115176. https://doi.org/10.1016/j.ssi.2019.115176.
[122] Gondolini A, Mercadelli E, Casadio S, Sanson A. Freeze cast support for hydrogen separation membrane. J Eur Ceram Soc 2022;42:1053–60. https://doi.org/10.1016/j.jeurceramsoc.2021.10.063.
[123] Gaudillere C, Serra JM. Freeze-casting: fabrication of highly porous and hierarchical ceramic supports for energy applications. Bol Soc Espanola Ceram Vidr 2016;55:45–54. https://doi.org/10.1016/j.bsecv.2016.02.002.
[124] Shao G, Hanaor DAH, Shen X, Gurlo A. Freeze casting: from low-Dimensional building blocks to aligned porous structures-A review of novel materials, methods, and applications. Adv Mater 2020;32:e1907176. https://doi.org/10.1002/adma.201907176.
[125] Liu R, Xu T, Wang C. A review of fabrication strategies and applications of porous ceramics prepared by freeze-casting method. Ceram Int 2016;42:2907–25. https://doi.org/10.1016/j.ceramint.2015.10.148.
[126] Scotti KL, Dunand DC. Freeze casting – a review of processing, microstructure and properties via the open data repository, FreezeCasting.net. Prog Mater Sci 2018; 94:243–305. https://doi.org/10.1016/j.pmatsci.2018.01.001.
[127] Gondolini A, Bartoletti A, Mercadelli E, Gramazio P, Fasolini A, Basile F, et al. Development and hydrogen permeation of freeze-cast ceramic membrane. J Membr Sci 2023;684:121865. https://doi.org/10.1016/j.memsci.2023.121865.
[128] Gaudillere C, Garcia-Fayos J, Balaguer M, Serra JM. Enhanced oxygen separation through robust freeze-cast bilayered dual-phase membranes. ChemSusChem 2014;7:2554–61. https://doi.org/10.1002/cssc.201402324.
[129] Gaudillere C, Garcia-Fayos J, Serra JM. Enhancing oxygen permeation through hierarchically-structured perovskite membranes elaborated by freeze-casting. J Mater Chem A 2014;2:3828–33. https://doi.org/10.1039/C3TA14069E.
[130] Zou Y, Gaudillere C, Escribano JE, Serra JM, Malzbender J. Microstructure, mechanical behavior and flow resistance of freeze-cast porous 3YSZ substrates for membrane applications. J Eur Ceram Soc 2017;37:3167–76. https://doi.org/10.1016/j.jeurceramsoc.2017.03.056.
[131] Schulze-Küppers F, Unije UV, Blank H, Balaguer M, Baumann S, Mücke R, et al. Comparison of freeze-dried and tape-cast support microstructure on high-flux oxygen transport membrane performance. J Membr Sci 2018;564:218–26. https://doi.org/10.1016/j.memsci.2018.07.028.
[132] Souza DF, Nunes EHM, Vasconcelos WL. Preparation of Ba0.5Sr0.5Co0.8Fe0.2O3−δ asymmetric structures by freeze-casting and dip-coating. Ceram Int 2018;44:1002–6. https://doi.org/10.1016/j.ceramint.2017.10.035.
[133] Rachadel PL, Souza DF, Nunes EHM, da Costa JCD, Vasconcelos WL, Hotza D. A novel route for manufacturing asymmetric BSCF-based perovskite structures by a combined tape and freeze casting method. J Eur Ceram Soc 2017;37:5249–57. https://doi.org/10.1016/j.jeurceramsoc.2017.04.035.
[134] Gaudillere C, Garcia-Fayos J, Plaza J, Serra JM. Ice-templating for the Elaboration of oxygen permeation asymmetric tubular membrane with radial oriented porosity. Ceramics 2019;2:246–59. https://doi.org/10.3390/ceramics2020020.
[135] Liu T, Chen Y, Fang S, Lei L, Wang Y, Ren C, et al. A dual-phase bilayer oxygen permeable membrane with hierarchically porous structure fabricated by freeze-drying tape-casting method. J Membr Sci 2016;520:354–63. https://doi.org/10.1016/j.memsci.2016.07.046.
[136] Liu T, Zhao W, Wang Y. Robust freeze-cast bilayer dual-phase oxygen transport membrane targeting chemical reactor application. ACS Appl Nano Mater 2018;1: 3774–8. https://doi.org/10.1021/acsanm.8b00990.
[137] Athayde DD, Souza DF, Silva AMA, Vasconcelos D, Nunes EHM, Diniz da Costa JC, et al. Review of perovskite ceramic synthesis and membrane preparation methods. Ceram Int 2016;42:6555–71. https://doi.org/10.1016/j.ceramint.2016.01.130.
[138] Lu X, Lee Y, Yang S, Hao Y, Evans JRG, Parini CG. Solvent-based paste extrusion solid freeforming. J Eur Ceram Soc 2010;30:1–10. https://doi.org/10.1016/j.jeurceramsoc.2009.07.019.
[139] Trunec M. Fabrication of zirconia- and ceria-based thin-wall tubes by thermoplastic extrusion. J Eur Ceram Soc 2004;24:645–51. https://doi.org/10.1016/S0955-2219(03)00258-9.
[140] Meng X, Yan W, Yang N, Tan X, Liu S. Highly stable microtubular solid oxide fuel cells based on integrated electrolyte/anode hollow fibers. J Power Sources 2015; 275:362–9. https://doi.org/10.1016/j.jpowsour.2014.11.027.
[141] Gurauskis J, Gil V, Lin B, Einarsrud M-A. Pilot scale fabrication of lanthanum tungstate supports for H2 separation membranes. Open Ceramics 2022;9:100226. https://doi.org/10.1016/j.oceram.2022.100226.
[142] Tan X, Tan X, Yang N, Meng B, Zhang K, Liu S. High performance BaCe0.8Y0.2O3−a (BCY) hollow fibre membranes for hydrogen permeation. Ceram Int 2014;40:3131–8. https://doi.org/10.1016/j.ceramint.2013.09.132.
[143] Song J, Kang J, Tan X, Meng B, Liu S. Proton conducting perovskite hollow fibre membranes with surface catalytic modification for enhanced hydrogen separation. J Eur Ceram Soc 2016;36:1669–77. https://doi.org/10.1016/j.jeurceramsoc.2016.01.006.
[144] Cheng H, Wang X, Meng X, Meng B, Sunarso J, Tan X, et al. Dual-layer BaCe0.8Y0.2O3-δ-Ce0.8Y0.2O2-δ/BaCe0.8Y0.2O3-δ-Ni hollow fiber membranes for H2 separation. J Membr Sci 2020;601:117801. https://doi.org/10.1016/j.memsci.2019.117801.
[145] Zhang C, Xu Z, Chang X, Zhang Z, Jin W. Preparation and characterization of mixed-conducting thin tubular membrane. J Membr Sci 2007;299:261–7. https://doi.org/10.1016/j.memsci.2007.05.001.
[146] Gromada M, Trawczyński J, Wierzbicki M, Zawadzki M. Effect of forming techniques on efficiency of tubular oxygen separating membranes. Ceram Int 2017;43:256–61. https://doi.org/10.1016/j.ceramint.2016.09.147.
[147] Hoffmann R, Pippardt U, Kriegel R. Impact of extrusion parameters on the mechanical performance of tubular BSCF-supports for asymmetric oxygen transporting membranes. J Membr Sci 2019;570–571:61–8. https://doi.org/10.1016/j.memsci.2018.10.019.
[148] Hoffmann R, Pippardt U, Kriegel R. Impact of sintering temperature on permeation and long-term development of support structure and stability for asymmetric oxygen transporting BSCF membranes. J Membr Sci 2019;581: 270–82. https://doi.org/10.1016/j.memsci.2019.03.066.
[149] Liu S, Gavalas GR. Preparation of oxygen ion conducting ceramic hollow-fiber membranes. Ind Eng Chem Res 2005;44:7633–7. https://doi.org/10.1021/ie040279i.
[150] Liu S, Gavalas GR. Oxygen selective ceramic hollow fiber membranes. J Membr Sci 2005;246:103–8. https://doi.org/10.1016/j.memsci.2004.09.028.
[151] Tian T, Li W, Liu T, Chen C. Preparation and oxygen permeability of Ce0.8Sm0.2O2−δ-La0.7Ca0.3CrO3−δ dual-phase composite hollow fiber membrane. Solid State Ionics 2012;225:690–4. https://doi.org/10.1016/j.ssi.2012.02.055.
[152] Ren C, Gan Y, Yang C, Lee M, Xue X. A rational asymmetric hollow fiber membrane for oxygen permeation. Int J Appl Ceram Technol 2019;16:791–801. https://doi.org/10.1111/ijac.13121.
[153] A rational asymmetric hollow fiber membrane for oxygen permeation - Ren - 2019 - International Journal of Applied Ceramic Technology - Wiley Online Library n.d. https://ceramics.onlinelibrary.wiley.com/doi/full/10.1111/ijac.13121 (accessed August 7, 2023).
[154] Bortzmeyer D. Dry pressing of ceramic powders. In: Terpstra RA, Pex PPAC, de Vries AH, editors. Ceramic processing. Dordrecht: Springer Netherlands; 1995. p. 102–46. https://doi.org/10.1007/978-94-011-0531-6_4.
[155] Ewsuk KG. Powder granulation and compaction. https://doi.org/10.1016/B0-08-043152-6/01401-7; 2001.
[156] Choi H, Cho GY, Cha S-W. Fabrication and characterization of anode supported YSZ/GDC bilayer electrolyte SOFC using dry press process. International Journal of Precision Engineering and Manufacturing-Green Technology 2014;1:95–9. https://doi.org/10.1007/s40684-014-0013-4.
[157] Chen P, Kim G-Y, Ni J. Investigations in the compaction and sintering of large ceramic parts. J Mater Process Technol 2007;190:243–50. https://doi.org/10.1016/j.jmatprotec.2007.02.039.
[158] Rebollo E, Mortalò C, Escolástico S, Boldrini S, Barison S, Serra JM, et al. Exceptional hydrogen permeation of all-ceramic composite robust membranes based on BaCe0.65Zr0.20Y0.15O3−δ and Y- or Gd-doped ceria. Energy Environ Sci 2015;8:3675–86. https://doi.org/10.1039/C5EE01793A.
[159] Cheng S, Gupta VK, Lin JYS. Synthesis and hydrogen permeation properties of asymmetric proton-conducting ceramic membranes. Solid State Ionics 2005;176: 2653–62. https://doi.org/10.1016/j.ssi.2005.07.005.
[160] Zhan S, Zhu X, Ji B, Wang W, Zhang X, Wang J, et al. Preparation and hydrogen permeation of SrCe0.95Y0.05O3−δ asymmetrical membranes. J Membr Sci 2009; 340:241–8. https://doi.org/10.1016/j.memsci.2009.05.037.
[161] Zhu Z, Yan L, Liu H, Sun W, Zhang Q, Liu W. A mixed electronic and protonic conducting hydrogen separation membrane with asymmetric structure. Int J Hydrogen Energy 2012;37:12708–13. https://doi.org/10.1016/j.ijhydene.2012.06.033.
[162] Wei Y, Xue J, Wang H, Caro J. Hydrogen permeability and stability of BaCe0.85Tb0.05Zr0.1O3−δ asymmetric membranes. J Membr Sci 2015;488: 173–81. https://doi.org/10.1016/j.memsci.2015.04.035.
[163] Weng G, Ouyang K, Lin X, Wen S, Zhou Y, Lei S, et al. Enhanced hydrogen permeability of mixed protonic–electronic conducting membranes through an in-Situ Exsolution strategy. Adv Funct Mater 2022;32:2205255. https://doi.org/10.1002/adfm.202205255.

[164] Chen Z, Shao Z, Ran R, Zhou W, Zeng P, Liu S. A dense oxygen separation membrane with a layered morphologic structure. J Membr Sci 2007;300:182–90. https://doi.org/10.1016/j.memsci.2007.05.023.
[165] Jiang Q, Nordheden KJ, Stagg-Williams SM. Oxygen permeation study and improvement of Ba0.5Sr0.5Co0.8Fe0.2Ox perovskite ceramic membranes. J Membr Sci 2011;369:174–81. https://doi.org/10.1016/j.memsci.2010.11.073.
[166] Kim J-H, Kang Y-M, Kim B-G, Lee S-H, Hwang K-T. Preparation of dense composite membrane with Ba-cerate conducting oxide and rapidly solidified Zr-based alloy. Int J Hydrogen Energy 2011;36:10129–35. https://doi.org/10.1016/j.ijhydene.2011.02.145.
[167] Zhang Z, Chen D, Chen Y, Hao Y, Tade MO, Shao Z. Facile fabrication and improved carbon dioxide tolerance of a novel bilayer-structured ceramic oxygen permeating membrane. J Membr Sci 2014;472:10–8. https://doi.org/10.1016/j.memsci.2014.08.039.
[168] Ishii K, Matsunaga C, Kobayashi K, Stevenson AJ, Tardivat C, Uchikoshi T. Fabrication of BSCF-based mixed ionic-electronic conducting membrane by electrophoretic deposition for oxygen separation application. J Eur Ceram Soc 2019;39:5292–7. https://doi.org/10.1016/j.jeurceramsoc.2019.07.051.
[169] Kiebach R, Pirou S, Aguilera LM, Haugen AB, Kaiser A, Hendriksen PV, et al. A review on dual-phase oxygen transport membranes: from fundamentals to commercial deployment. Journal Materials Chemistry A 2022;10:2152–95. https://doi.org/10.1039/D1TA07898D.
[170] Mu S, Hong Y, Huang H, Ishii A, Lei J, Song Y, et al. A novel Laser 3D printing method for the advanced manufacturing of protonic ceramics. Membranes 2020;10:98. https://doi.org/10.3390/membranes10050098.
[171] Bartoletti A, Sangiorgi A, Gondolini A, Mercadelli E, Casadio S, García-González S, et al. Dispersant- and solvent-free pastes for UV-assisted micro-extrusion of porous proton conductive membrane supports. J Eur Ceram Soc 2023;43:4844–53. https://doi.org/10.1016/j.jeurceramsoc.2023.04.038.
[172] Bartoletti A, Sangiorgi A, Mercadelli E, Melandri C, Gondolini A, García-González S, et al. 3D microextrusion of eco-friendly water based cer-cer composite pastes for hydrogen separation. Open Ceramics 2023;16:100504. https://doi.org/10.1016/j.oceram.2023.100504.